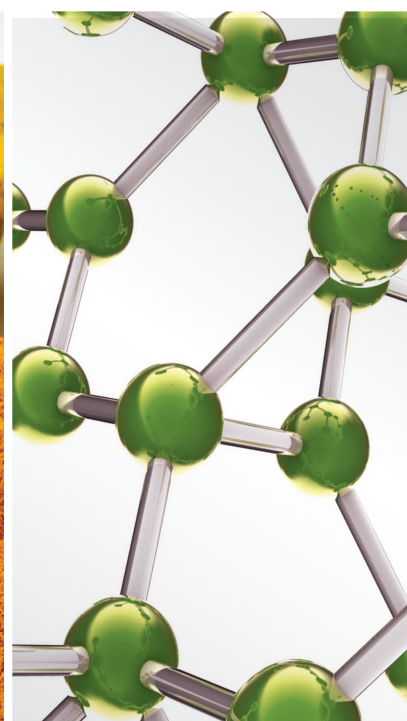
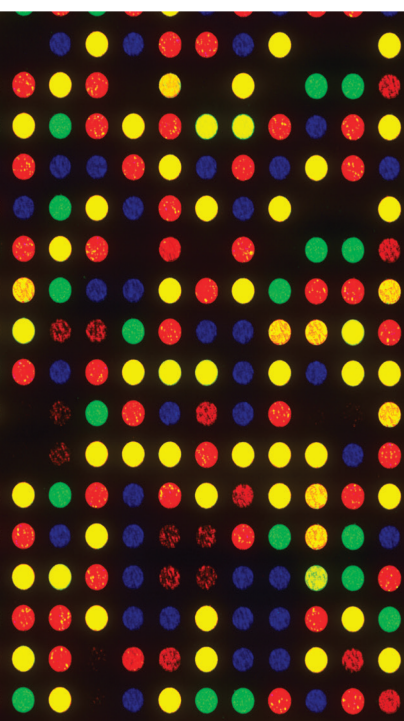


Nanodelivery Techniques for Natural Products for Improving Efficacy

Lead Guest Editor: Muhammad Taher

Guest Editors: Heni Rachmawati, Deny Susanti, and Md. Atiar Rahman





Nanodelivery Techniques for Natural Products for Improving Efficacy

Nanodelivery Techniques for Natural Products for Improving Efficacy

Lead Guest Editor: Muhammad Taher

Guest Editors: Heni Rachmawati, Deny Susanti,
and Md. Atiar Rahman



Copyright © 2021 Hindawi Limited. All rights reserved.

This is a special issue published in "Evidence-Based Complementary and Alternative Medicine." All articles are open access articles distributed under the Creative Commons Attribution License, which permits unrestricted use, distribution, and reproduction in any medium, provided the original work is properly cited.

Chief Editor

Jian-Li Gao , China






Associate Editors

Hyunsu Bae , Republic of Korea
Raffaele Capasso , Italy
Jae Youl Cho , Republic of Korea
Caigan Du , Canada
Yuewen Gong , Canada
Hai-dong Guo , China
Kuzhuvelil B. Harikumar , India
Ching-Liang Hsieh , Taiwan
Cheorl-Ho Kim , Republic of Korea
Victor Kuete , Cameroon
Hajime Nakae , Japan
Yoshiji Ohta , Japan
Olumayokun A. Olajide , United Kingdom
Chang G. Son , Republic of Korea
Shan-Yu Su , Taiwan
Michał Tomczyk , Poland
Jenny M. Wilkinson , Australia

Academic Editors

Eman A. Mahmoud , Egypt
Ammar AL-Farga , Saudi Arabia
Smail Aazza , Morocco
Nahla S. Abdel-Azim, Egypt
Ana Lúcia Abreu-Silva , Brazil
Gustavo J. Acevedo-Hernández , Mexico
Mohd Adnan , Saudi Arabia
Jose C Adsuar , Spain
Sayeed Ahmad, India
Touqeer Ahmed , Pakistan
Basiru Ajiboye , Nigeria
Bushra Akhtar , Pakistan
Fahmida Alam , Malaysia
Mohammad Jahoor Alam, Saudi Arabia
Clara Albani, Argentina
Ulysses Paulino Albuquerque , Brazil
Mohammed S. Ali-Shtayeh , Palestinian Authority
Ekram Alias, Malaysia
Terje Alraek , Norway
Adolfo Andrade-Cetto , Mexico
Letizia Angiolella , Italy
Makoto Arai , Japan

Daniel Dias Rufino Arcanjo , Brazil
Duygu AĞAGÜNDÜZ , Turkey
Neda Baghban , Iran
Samra Bashir , Pakistan
Rusliza Basir , Malaysia
Jairo Kenupp Bastos , Brazil
Arpita Basu , USA
Mateus R. Beguelini , Brazil
Juana Benedí, Spain
Samira Boulbaroud, Morocco
Mohammed Bourhia , Morocco
Abdelhakim Bouyahya, Morocco
Nunzio Antonio Cacciola , Italy
Francesco Cardini , Italy
María C. Carpinella , Argentina
Harish Chandra , India
Guang Chen, China
Jianping Chen , China
Kevin Chen, USA
Mei-Chih Chen, Taiwan
Xiaojia Chen , Macau
Evan P. Cherniack , USA
Giuseppina Chianese , Italy
Kok-Yong Chin , Malaysia
Lin China, China
Salvatore Chirumbolo , Italy
Hwi-Young Cho , Republic of Korea
Jeong June Choi , Republic of Korea
Jun-Yong Choi, Republic of Korea
Kathrine Bisgaard Christensen , Denmark
Shuang-En Chuang, Taiwan
Ying-Chien Chung , Taiwan
Francisco José Cidral-Filho, Brazil
Daniel Collado-Mateo , Spain
Lisa A. Conboy , USA
Kieran Cooley , Canada
Edwin L. Cooper , USA
José Otávio do Amaral Corrêa , Brazil
Maria T. Cruz , Portugal
Huantian Cui , China
Giuseppe D'Antona , Italy
Ademar A. Da Silva Filho , Brazil
Chongshan Dai, China
Laura De Martino , Italy
Josué De Moraes , Brazil

Arthur De Sá Ferreira , Brazil
Nunziatina De Tommasi , Italy
Marinella De leo , Italy
Gourav Dey , India
Dinesh Dhamecha, USA
Claudia Di Giacomo , Italy
Antonella Di Sotto , Italy
Mario Dioguardi, Italy
Jeng-Ren Duann , USA
Thomas Effërth , Germany
Abir El-Alfy, USA
Mohamed Ahmed El-Esawi , Egypt
Mohd Ramli Elvy Suhana, Malaysia
Talha Bin Emran, Japan
Roger Engel , Australia
Karim Ennouri , Tunisia
Giuseppe Esposito , Italy
Tahereh Eteraf-Oskouei, Iran
Robson Xavier Faria , Brazil
Mohammad Fattahi , Iran
Keturah R. Faurot , USA
Piergiorgio Fedeli , Italy
Laura Ferraro , Italy
Antonella Fioravanti , Italy
Carmen Formisano , Italy
Hua-Lin Fu , China
Liz G Müller , Brazil
Gabino Garrido , Chile
Safoora Gharibzadeh, Iran
Muhammad N. Ghayur , USA
Angelica Gomes , Brazil
Elena González-Burgos, Spain
Susana Gorzalczany , Argentina
Jiangyong Gu , China
Maruti Ram Gudavalli , USA
Jian-You Guo , China
Shanshan Guo, China
Narcís Gusi , Spain
Svein Haavik, Norway
Fernando Hallwass, Brazil
Gajin Han , Republic of Korea
Ihsan Ul Haq, Pakistan
Hicham Harhar , Morocco
Mohammad Hashem Hashempur , Iran
Muhammad Ali Hashmi , Pakistan

Waseem Hassan , Pakistan
Sandrina A. Heleno , Portugal
Pablo Herrero , Spain
Soon S. Hong , Republic of Korea
Md. Akil Hossain , Republic of Korea
Muhammad Jahangir Hossen , Bangladesh
Shih-Min Hsia , Taiwan
Changmin Hu , China
Tao Hu , China
Weicheng Hu , China
Wen-Long Hu, Taiwan
Xiao-Yang (Mio) Hu, United Kingdom
Sheng-Teng Huang , Taiwan
Ciara Hughes , Ireland
Attila Hunyadi , Hungary
Liaqat Hussain , Pakistan
Maria-Carmen Iglesias-Osma , Spain
Amjad Iqbal , Pakistan
Chie Ishikawa , Japan
Angelo A. Izzo, Italy
Satveer Jagwani , USA
Rana Jamous , Palestinian Authority
Muhammad Saeed Jan , Pakistan
G. K. Jayaprakasha, USA
Kyu Shik Jeong, Republic of Korea
Leopold Jirovetz , Austria
Jeeyoun Jung , Republic of Korea
Nurkhalida Kamal , Saint Vincent and the
Grenadines
Atsushi Kameyama , Japan
Kyungsu Kang, Republic of Korea
Wenyi Kang , China
Shao-Hsuan Kao , Taiwan
Nasiara Karim , Pakistan
Morimasa Kato , Japan
Kumar Katragunta , USA
Deborah A. Kennedy , Canada
Washim Khan, USA
Bonglee Kim , Republic of Korea
Dong Hyun Kim , Republic of Korea
Junghyun Kim , Republic of Korea
Kyungho Kim, Republic of Korea
Yun Jin Kim , Malaysia
Yoshiyuki Kimura , Japan

Nebojša Kladar , Serbia
Mi Mi Ko , Republic of Korea
Toshiaki Kogure , Japan
Malcolm Koo , Taiwan
Yu-Hsiang Kuan , Taiwan
Robert Kubina , Poland
Chan-Yen Kuo , Taiwan
Kuang C. Lai , Taiwan
King Hei Stanley Lam, Hong Kong
Faniel Lampiao, Malawi
Ilaria Lampronti , Italy
Mario Ledda , Italy
Harry Lee , China
Jeong-Sang Lee , Republic of Korea
Ju Ah Lee , Republic of Korea
Kyu Pil Lee , Republic of Korea
Namhun Lee , Republic of Korea
Sang Yeoup Lee , Republic of Korea
Ankita Leekha , USA
Christian Lehmann , Canada
George B. Lenon , Australia
Marco Leonti, Italy
Hua Li , China
Min Li , China
Xing Li , China
Xuqi Li , China
Yi-Rong Li , Taiwan
Vuanghao Lim , Malaysia
Bi-Fong Lin, Taiwan
Ho Lin , Taiwan
Shuibin Lin, China
Kuo-Tong Liou , Taiwan
I-Min Liu, Taiwan
Suhuan Liu , China
Xiaosong Liu , Australia
Yujun Liu , China
Emilio Lizarraga , Argentina
Monica Loizzo , Italy
Nguyen Phuoc Long, Republic of Korea
Zaira López, Mexico
Chunhua Lu , China
Ângelo Luís , Portugal
Anderson Luiz-Ferreira , Brazil
Ivan Luzardo Luzardo-Ocampo, Mexico

Michel Mansur Machado , Brazil
Filippo Maggi , Italy
Juraj Majtan , Slovakia
Toshiaki Makino , Japan
Nicola Malafronte, Italy
Giuseppe Malfa , Italy
Francesca Mancianti , Italy
Carmen Mannucci , Italy
Juan M. Manzanque , Spain
Fatima Martel , Portugal
Carlos H. G. Martins , Brazil
Maulidiani Maulidiani, Malaysia
Andrea Maxia , Italy
Avijit Mazumder , India
Isac Medeiros , Brazil
Ahmed Mediani , Malaysia
Lewis Mehl-Madrona, USA
Ayikoé Guy Mensah-Nyagan , France
Oliver Micke , Germany
Maria G. Miguel , Portugal
Luigi Milella , Italy
Roberto Miniero , Italy
Letteria Minutoli, Italy
Prashant Modi , India
Daniel Kam-Wah Mok, Hong Kong
Changjong Moon , Republic of Korea
Albert Moraska, USA
Mark Moss , United Kingdom
Yoshiharu Motoo , Japan
Yoshiki Mukudai , Japan
Sakthivel Muniyan , USA
Saima Muzammil , Pakistan
Benoit Banga N'guessan , Ghana
Massimo Nabissi , Italy
Siddavaram Nagini, India
Takao Namiki , Japan
Srinivas Nammi , Australia
Krishnadas Nandakumar , India
Vitaly Napadow , USA
Edoardo Napoli , Italy
Jorddy Neves Cruz , Brazil
Marcello Nicoletti , Italy
Eliud Nyaga Mwaniki Njagi , Kenya
Cristina Nogueira , Brazil

Sakineh Kazemi Noureini , Iran
Rômulo Dias Novaes, Brazil
Martin Offenbaecher , Germany
Oluwafemi Adeleke Ojo , Nigeria
Olufunmiso Olusola Olajuyigbe , Nigeria
Luís Flávio Oliveira, Brazil
Mozaniel Oliveira , Brazil
Atolani Olubunmi , Nigeria
Abimbola Peter Oluyori , Nigeria
Timothy Omara, Austria
Chiagoziem Anariochi Otuechere , Nigeria
Sokcheon Pak , Australia
Antônio Palumbo Jr, Brazil
Zongfu Pan , China
Siyaram Pandey , Canada
Niranjan Parajuli , Nepal
Gunhyuk Park , Republic of Korea
Wansu Park , Republic of Korea
Rodolfo Parreira , Brazil
Mohammad Mahdi Parvizi , Iran
Luiz Felipe Passero , Brazil
Mitesh Patel, India
Claudia Helena Pellizzon , Brazil
Cheng Peng, Australia
Weijun Peng , China
Sonia Piacente, Italy
Andrea Pieroni , Italy
Haifa Qiao , USA
Cláudia Quintino Rocha , Brazil
DANIELA RUSSO , Italy
Muralidharan Arumugam Ramachandran,
Singapore
Manzoor Rather , India
Miguel Rebollo-Hernanz , Spain
Gauhar Rehman, Pakistan
Daniela Rigano , Italy
José L. Rios, Spain
Francisca Rius Diaz, Spain
Eliana Rodrigues , Brazil
Maan Bahadur Rokaya , Czech Republic
Mariangela Rondanelli , Italy
Antonietta Rossi , Italy
Mi Heon Ryu , Republic of Korea
Bashar Saad , Palestinian Authority
Sabi Saheed, South Africa

Mohamed Z.M. Salem , Egypt
Avni Sali, Australia
Andreas Sandner-Kiesling, Austria
Manel Santafe , Spain
José Roberto Santin , Brazil
Tadaaki Satou , Japan
Roland Schoop, Switzerland
Sindy Seara-Paz, Spain
Veronique Seidel , United Kingdom
Vijayakumar Sekar , China
Terry Selfe , USA
Arham Shabbir , Pakistan
Suzana Shahar, Malaysia
Wen-Bin Shang , China
Xiaofei Shang , China
Ali Sharif , Pakistan
Karen J. Sherman , USA
San-Jun Shi , China
Insop Shim , Republic of Korea
Maria Im Hee Shin, China
Yukihiro Shoyama, Japan
Morry Silberstein , Australia
Samuel Martins Silvestre , Portugal
Preet Amol Singh, India
Rajeev K Singla , China
Kuttulebbai N. S. Sirajudeen , Malaysia
Slim Smaoui , Tunisia
Eun Jung Sohn , Republic of Korea
Maxim A. Solovchuk , Taiwan
Young-Jin Son , Republic of Korea
Chengwu Song , China
Vanessa Steenkamp , South Africa
Annarita Stringaro , Italy
Keiichiro Sugimoto , Japan
Valeria Sulsen , Argentina
Zewei Sun , China
Sharifah S. Syed Alwi , United Kingdom
Orazio Tagliatalata-Scafati , Italy
Takashi Takeda , Japan
Gianluca Tamagno , Ireland
Hongxun Tao, China
Jun-Yan Tao , China
Lay Kek Teh , Malaysia
Norman Temple , Canada

Kamani H. Tennekoon , Sri Lanka
Seong Lin Teoh, Malaysia
Menaka Thounaojam , USA
Jinhui Tian, China
Zipora Tietel, Israel
Loren Toussaint , USA
Riaz Ullah , Saudi Arabia
Philip F. Uzor , Nigeria
Luca Vanella , Italy
Antonio Vassallo , Italy
Cristian Vergallo, Italy
Miguel Vilas-Boas , Portugal
Aristo Vojdani , USA
Yun WANG , China
QIBIAO WU , Macau
Abraham Wall-Medrano , Mexico
Chong-Zhi Wang , USA
Guang-Jun Wang , China
Jinan Wang , China
Qi-Rui Wang , China
Ru-Feng Wang , China
Shu-Ming Wang , USA
Ting-Yu Wang , China
Xue-Rui Wang , China
Youhua Wang , China
Kenji Watanabe , Japan
Jintanaporn Wattanathorn , Thailand
Silvia Wein , Germany
Katarzyna Winska , Poland
Sok Kuan Wong , Malaysia
Christopher Worsnop, Australia
Jih-Huah Wu , Taiwan
Sijin Wu , China
Xian Wu, USA
Zuoqi Xiao , China
Rafael M. Ximenes , Brazil
Guoqiang Xing , USA
JiaTuo Xu , China
Mei Xue , China
Yong-Bo Xue , China
Haruki Yamada , Japan
Nobuo Yamaguchi, Japan
Junqing Yang, China
Longfei Yang , China

Mingxiao Yang , Hong Kong
Qin Yang , China
Wei-Hsiung Yang, USA
Swee Keong Yeap , Malaysia
Albert S. Yeung , USA
Ebrahim M. Yimer , Ethiopia
Yoke Keong Yong , Malaysia
Fadia S. Youssef , Egypt
Zhilong Yu, Canada
RONGJIE ZHAO , China
Sultan Zahiruddin , USA
Armando Zarrelli , Italy
Xiaobin Zeng , China
Y Zeng , China
Fangbo Zhang , China
Jianliang Zhang , China
Jiu-Liang Zhang , China
Mingbo Zhang , China
Jing Zhao , China
Zhangfeng Zhong , Macau
Guoqi Zhu , China
Yan Zhu , USA
Suzanna M. Zick , USA
Stephane Zingue , Cameroon

Contents

PEI-PEG-Coated Mesoporous Silica Nanoparticles Enhance the Antitumor Activity of Tanshinone IIA and Serve as a Gene Transfer Vector

Yinxing Zhu , Miao Yue , Ting Guo , Fang Li , Zhifeng Li , Dazhuang Yang , and Mei Lin 
Research Article (12 pages), Article ID 6756763, Volume 2021 (2021)

Microencapsulated Recombinant Human Epidermal Growth Factor Ameliorates Osteoarthritis in a Murine Model

Shih-Chao Lin , Xiang Zhang, Shiow-Yi Chen , Chi-Chien Lin , and Yen-Shuo Chiu 
Research Article (10 pages), Article ID 9163279, Volume 2021 (2021)

Research Article

PEI-PEG-Coated Mesoporous Silica Nanoparticles Enhance the Antitumor Activity of Tanshinone IIA and Serve as a Gene Transfer Vector

Yinxing Zhu ¹, Miao Yue ¹, Ting Guo ², Fang Li ¹, Zhifeng Li ², Dazhuang Yang ²,
and Mei Lin ³

¹Nanjing University of Chinese Medicine, Nanjing, Jiangsu 210023, China

²Institute of Clinical Medicine, Taizhou People's Hospital Affiliated to Nantong University, Taizhou, Jiangsu 225300, China

³Clinical Laboratory, Taizhou People's Hospital Affiliated to Nanjing University of Chinese Medicine, Taizhou, Jiangsu 225300, China

Correspondence should be addressed to Mei Lin; L_mei@163.com

Received 21 July 2021; Revised 22 September 2021; Accepted 21 October 2021; Published 8 November 2021

Academic Editor: Muhammad Taher

Copyright © 2021 Yinxing Zhu et al. This is an open access article distributed under the Creative Commons Attribution License, which permits unrestricted use, distribution, and reproduction in any medium, provided the original work is properly cited.

Tanshinone IIA (TanIIA) and gene therapy both hold promising potentials in hepatocellular carcinoma (HCC) treatment. However, low solubility and poor bioavailability of TanIIA limit its clinical application. Similarly, gene therapy with GPC3-shRNA, a type of short hairpin RNAs (shRNAs) capable of silencing the glypican-3 (GPC3) expression, is seriously limited due to its susceptibility to nuclease degradation and high off-target effects. In the present study, polyethyleneimine (PEI)-polyethylene glycol (PEG)-coated mesoporous silica nanoparticles (MSN-PEG) were used as a drug carrier. By encapsulating TanIIA into MSN-PEG, we synthesized MSN-TanIIA-PEG nanoparticles and observed the involved characteristics. This was followed by exploration of antitumor activity on the HepG2 cell lines *in vitro*. Meanwhile, in order to construct GPC3-shRNA plasmids, a shRNA sequence targeting GPC3 was synthesized and cloned into the pSLenti-U6 vector. Accordingly, the performance of MSN-PEG as a gene transfer carrier for GPC3-shRNA gene therapy of HCC *in vitro* was evaluated, including transfection efficiency and DNA binding biological characteristics. The results indicated successful encapsulation of TanIIA in MSN-PEG, which had satisfactory efficacy, favorable dispersity, suitable particle size, and sustained release effect. The *in vitro* anti-HCC effects of nano-TanIIA were greatly improved, which outperformed free-TanIIA in terms of proliferation and invasion inhibition, as well as apoptosis induction of HCC cells. As expected, MSN-PEG possessed excellent gene delivery capacity with good binding, release, and protection from RNase digestion. Using MSN-PEG as a gene carrier, the plasmids were successfully transfected into HepG2 cells, and both the mRNA and protein expressions of GPC3 were significantly downregulated. It was thus concluded that a sustained release TanIIA delivery system for HCC treatment was synthesized and that MSN-PEG could also serve as a gene transfer carrier for gene therapy. More interestingly, MSN-PEG may be a potential delivery platform that combines TanIIA and GPC3-shRNA together to enhance their synergistic effect.

1. Introduction

Hepatocellular carcinoma (HCC), as a malignancy characterized by high incidence and mortality, harms people's life and health in a tremendous manner. Seriously, its mortality and morbidity have been steadily increasing over the last few decades [1]. To date, chemotherapy remains the most common treatment for all stages of carcinoma patients. However, several potential chemotherapeutics that

can treat HCC still show limitations such as severe adverse reactions and drug resistance [2]. Moreover, the intricacy of the molecular pathogenesis poses great difficulties in seeking cure. Enormous endeavors have thus been made to develop high-efficacy multitarget antineoplastics with less adverse effects.

Several effective plant constituents, which are used in traditional Chinese medicine with insignificant adverse actions, have aroused a wide range of interest as an adjuvant

therapy [3]. Among them, TanIIA, an effective component extracted from the *Salvia miltiorrhiza* roots, features high efficacy, natural source, and low toxicity [4]. Based on the existing studies on TanIIA, it exerts a broad spectrum of antitumor activities in a variety of human carcinoma cells by suppressing proliferation and migration, triggering autophagy and apoptosis, and reversing the multidrug resistance [5]. Additionally, TanIIA has a synergistic effect in combination with other chemotherapeutics commonly used in clinics, which makes its application in the cancer and adjuvant therapies promising and offers a new insight into diverse cancer treatments as well [6].

Unsatisfactorily, being a lipophilic constituent, TanIIA is poorly bioavailable, which limits its further application [7]. Due to poor water solubility, it exhibits robust hepatic elimination after oral medication and can be easily eliminated from the circulatory system after intravenous medication [8, 9]. Hence, diverse delivery systems (nanoscale) have been proposed for controlled release of TanIIA, in order to overcome its disadvantages and to elevate its bioavailability [2, 9].

Amongst various nano-based drug delivery platforms developed, mesoporous silica nanoparticles (MSNs) have attracted a considerable attention owing to their good biocompatibility, monodispersity, feeble toxicity, tunable pore size, and large pore volumes, among other characteristics [10]. Despite being in part a potential solution to the foregoing problems with TanIIA, it still cannot escape the influence of the reticuloendothelial system (RES). Rapid elimination by the RES will inevitably hamper the nanosized drugs' absorption efficiency in tumor regions, leading to reduced bioavailability [11]. Being highly hydrophilic and positively charged, PEG is commonly used to decorate nanoparticles [12], which has been proven as one of the most effective methods to improve nanoparticle biodistribution and reduce opsonization by the RES [11].

Studies over the last decades have demonstrated that GPC3 is highly and specifically expressed in HCC, revealing its potential from an encouraging biomarker for the early HCC detection to an effective epitope for targeted HCC treatment. Past several years have witnessed the exploration of the GPC3-targeting gene therapies [13, 14]. As promising as it looks, their applications are severely limited because of the physicochemical traits of nucleotide drugs, including high molecular weight, susceptibility to nuclease degradation, easy missing of target, and anionic charge [15]. This has necessitated carrier design as the gene therapy advances in order to achieve highly efficient drug delivery to the target cells. ShRNAs, the small molecules of RNA, have specific function of gene silencing, which can be delivered to the targets via the support of nanoparticles [16]. Recently, nanostructured carriers such as PEG and PEI or inorganic nanoparticles have shown multiple advantages concerning RNA interference (RNAi) delivery [17]. PEI, as one of the most classic nonviral vectors, is the most broadly applied polycation transfection reagent owing to its high stability and transfection performance, while PEI-25k has been considered the gold standard for nonviral vectors [18, 19]. Moreover, PEI combined with PEG could improve the systemic circulation and prolong the treatment time [19, 20].

Based on the aforementioned theory, this study aims to construct an intelligent nanoplatform to improve the water solubility and bioavailability of TanIIA, which also serves as a vehicle of GPC3-shRNA. Herein, we propose a facile method, where TanIIA was physically adsorbed by mesoporous silica and then surface-modified with PEI-PEG to make it positively charged. In this way, the stability of the complex can be improved, which is conducive to loading GPC3-shRNA plasmids. The physicochemical property elucidation of the complex was accomplished, *in vitro* antitumor activities were investigated, and the feasibility of MSN-PEG as a GPC3-shRNA carrier was explored. Finally, we found that this novel drug delivery system is promising for HCC treatment. Figure 1 is a schematic illustration of the preparation of MSN-PEG nanoparticles and their delivery.

2. Materials and Methods

2.1. Materials, Reagents, and Cell Culture. TanIIA (purity $\geq 98\%$ by HPLC) was purchased from Shanghai Yuanye Biotech, Ltd. (Shanghai, China). Monodisperse mesoporous silica nanoparticles (MSNs) were provided by Nanoeast Biotech (Nanjing, China), which are a kind of inorganic nanomaterials with a highly ordered mesoporous structure, good chemical and thermal stability, and a large number of easily modified hydroxyl functional groups on the surface. PEG5k-PEI25k was provided by Tanshui Biotech (Shenzhen, China). The Annexin V-Alexa Fluor 647/PI Apoptosis Assay kit was purchased from FcMACS (Nanjing, China). Lipofectamine 2000, Tango Buffer, and DNase-I enzyme were purchased from Solarbio (Beijing, China). Cell counting kit-8 (CCK-8) was obtained from Beyotime Biotech (Shanghai, China). Fluorescent Hoechst 33342, crystal violet, and the rest of the reagents were purchased from Sangon Biotech (Shanghai, China).

The human HepG2 hepatocellular cancer cell line was obtained from the Shanghai Institute of Cell Research, Chinese Academy of Sciences (Shanghai, China). HepG2 cells were inoculated in Dulbecco's modified Eagle's medium (DMEM) (GIBCO, US) containing 10% fetal bovine serum (GIBCO, US) and supplemented with streptomycin and penicillin (GIBCO, US). The cells were cultured at 37°C in a humidified environment with 5% CO₂.

2.2. Preparation of the Nanoparticles. The MSN-TanIIA-PEG was prepared according to a film dispersion-ultrasonic method in the published articles [9, 21]. The first step was preparation of TanIIA-loaded MSNs. 5 mg MSN (25 mg/mL) and 500 μ g TanIIA (10 mg/mL) were mixed evenly in ethanol, and then 100 μ L of water was added slowly into the above solution under ultrasonic condition followed by 2-h incubation in a 37°C shaker. Finally, centrifugation was carried out at 10,000 rpm for 15 min to remove the residual solvent, so as to obtain the required sample (denoted as MSN-TanIIA), which was dried in a 45°C vacuum for 12 h and then stored at 4°C.

The next step was coating of the prepared MSN-TanIIA with PEI-PEG. In a nutshell, 5 mg MSN-TanIIA (10 mg/mL) was dripped into 20 mg (50 mg/mL) PEI-PEG followed by

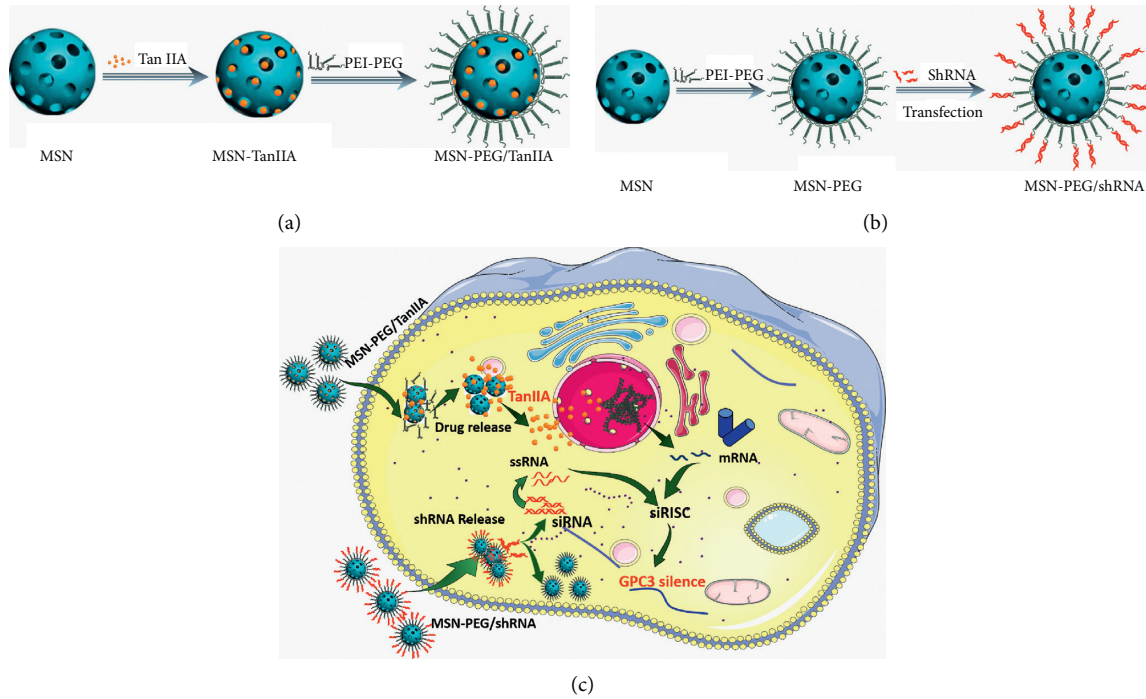


FIGURE 1: Schematic illustration of the preparation of MSN-PEG nanoparticles and their delivery. (a) Schematic of MSN-TanIIA-PEG preparation. (b) Schematic of MSN-PEG/shRNA preparation. (c) Schematic illustration of the proposed delivery of TanIIA and GPC3-shRNA transfected by MSN-PEG for a synergistic effect *in vitro*. The MSN-TanIIA-PEG and MSN-PEG/GPC3-shRNA nanocomplexes accumulate in the tumor via the EPR effect followed by cellular uptake by endocytosis. TanIIA and GPC3-shRNA are released from the nanocomplexes into the cytoplasm. Then, TanIIA enters into the nucleus, and GPC3-shRNA breaks into siRNAs and siRNA targets to degrade GPC3 mRNA under the assistance of siRISC. Abbreviations: EPR: enhanced permeability and retention, RISC: RNA-induced silencing complex.

probe sonication for 20 min. After removing extra PEI-PEG and free-TanIIA in the solution via 10-min centrifugation (10,000 rpm), the remaining was washed three times in 2 mL of saline via 5-min centrifugation (10,000 rpm) to get TanIIA-loaded PEI-PEG-coated MSNs, denoted as MSN-TanIIA-PEG. Meanwhile, MSN-PEG was also prepared by the same method.

The entrapped TanIIA in the obtained sample solution was quantified by HPLC. The drug loading capacity (DL, %) and encapsulation efficiency (EE, %) were calculated by the following equations:

$$DL (\%) = \left(\frac{\text{amount of TanIIA encapsulated in NPs}}{\text{total amount of NPs}} \right) \times 100,$$

$$EE (\%) = \left(\frac{\text{amount of TanIIA loaded in NPs}}{\text{initial TanIIA added}} \right) \times 100.$$

(1)

2.3. HPLC Method for Determining TanIIA

2.3.1. Instruments and Conditions. Taking the Chinese Pharmacopoeia (2020 edition) and Liu et al.'s research as reference [22], the high-performance liquid chromatography (HPLC) system (LC-15C; Shimadzu, Japan) with a

WondaSil C18 column (4.6 × 250 mm, 5 μm) was used for determination of TanIIA in MSN-TanIIA and MSN-TanIIA-PEG. In addition, the mobile phase of the HPLC system consisted of 70% acetonitrile (A) and 30% ultrapure water (B) at a flow rate of 1 mL/min, column temperature was kept at 30°C, and the detection wavelength was 268 nm.

2.3.2. Standard Solution and Sample Preparation. TanIIA standard solutions (1 mg/mL) were prepared in acetonitrile and stored at -20°C until use. Mobile phase was used to dilute standard solutions to the concentrations of 6.25, 12.5, 25, 50, and 100 μg/mL. Acetonitrile was used to break down the internal structure of the samples, thereby extracting the TanIIA before detecting [23, 24].

2.4. Characterization of the Nanoparticles. The physical and chemical properties of MSN-TanIIA-PEG were characterized by transmission electron microscopy (TEM), zeta potential, and dynamic light scattering (DLS). The particle size (nm) and zeta potential (mV) of nanoparticles were evaluated by dynamic light scattering (DLS) at 25°C using the Zeta Plus Zetasizer (Brookhaven Instruments, USA). All the samples were dispersed in deionized water and sonicated before the analysis. The morphology of the uncoated and coated nanoparticles was observed by a JEM-2100 TEM instrument (JEOL, Japan).

2.5. *In Vitro* Drug Release. A dialysis technique was employed for the release profile investigation of TanIIA from MSN-TanIIA and MSN-TanIIA-PEG. Initially, 1 mL of the sample solution (1 mg/mL) was added to a dialysis bag (MW: 3500), which was soaked in 5 mL of PBS buffer (0.02 M, pH = 7.4, containing 0.2% Tween-80), followed by stirring in a shaking bed at 100 rpm and 37°C away from light. At the preset points of time, each 1.0 mL of sample was removed from the release medium, and then the system was replenished with an equal volume of PBS. The HPLC was finally employed to examine how much TanIIA was released into the release solution.

2.6. *In Vitro* Antitumor Activity. To investigate the antitumor activity of MSN-TanIIA-PEG, *in vitro* proliferation, apoptosis, and invasion were assessed (see Sections 2.6.1/2.6.2/2.6.3/2.6.4).

2.6.1. CCK-8 Assay. A CCK-8 assay was conducted to determine the cell proliferation inhibitory effect of the three different TanIIA formulations (free-TanIIA, TanIIA-MSN, and MSN-TanIIA-PEG) on HepG2 cells. In brief, the 3×10^4 cells were seeded into 96-well plates overnight. Then, the cells were intervened with a series of different concentrations (0, 1.25, 2.5, 5, 10, 20, 40, and 80 $\mu\text{g/mL}$) of free-TanIIA, TanIIA-MSN, and MSN-TanIIA-PEG for 24 h. DMSO was used as a solvent for TanIIA, and thus the HepG2 cells in DMEM containing 0.3% DMSO were used as the untreated control group (0 $\mu\text{g/mL}$). Moreover, MSN-PEG was also used as a blank nanoparticle control. Subsequently, 10 μL of CCK-8 reagent was added to each well, and the cells were incubated for 30 min at 37°C according to the manufacturer's protocol. Finally, the absorbance was measured using a microplate reader (Thermo Scientific, USA) at a wavelength of 450 nm. The cell growth inhibition rate of the HepG2 cells was calculated according to the formula: cell growth inhibition rate (%) = $(1 - \text{experimental absorbance value} / \text{control absorbance value}) \times 100$. The 50% inhibitory concentrations (IC_{50}) were determined using GraphPad Prism 8.0 software (La Jolla, USA).

2.6.2. Hoechst 33342 Staining Assay. After seeding into 24-well plates overnight, HepG2 cells (1×10^5 cells) were intervened with free-TanIIA, MSN-TanIIA, and MSN-TanIIA-PEG at an equivalent TanIIA concentration of 10 $\mu\text{g/mL}$. Besides, the concentration of MSN-PEG in the MSN-PEG group was 100 $\mu\text{g/mL}$. After additional 24-h incubation at 37°C, the cells were washed with cold PBS. Hoechst 33342 (1 $\mu\text{g/mL}$) was added to each well. After being incubated at 37°C for 15 min, the cells were visualized under a fluorescence microscope (Leica, Germany).

2.6.3. Flow Cytometry Analysis. Before the intervention, the cells were inoculated at 4×10^5 cells per well in 6-well plates overnight. Afterward, the cells were intervened with MSN-PEG (100 $\mu\text{g/mL}$), free-TanIIA, MSN-TanIIA, and MSN-

TanIIA-PEG (at an equivalent TanIIA concentration of 10 $\mu\text{g/mL}$) for 24 h.

For apoptosis detection, the cells were collected and PBS-washed followed by staining with Annexin V-Alexa Fluor 647 (5 μL) and PI (10 μL , 20 $\mu\text{g/mL}$) at room temperature protected from light for 15 min and a subsequent resuspension in 500 μL of binding buffer (10 mM HEPES/NaOH, pH 7.4, 140 mM NaCl, 2.5 mM CaCl_2). The stained cells were detected immediately using FACSCalibur (BD Biosciences, USA).

For the cell cycle assessment, the cells were harvested, PBS-washed, and fixed overnight at 4°C in cold 70% ethanol. After collecting and washing with PBS, the cells were stained using propidium iodide (PI) solution (100 μL ; 20 $\mu\text{g/mL}$ PI and 5 $\mu\text{g/mL}$ RNase A in PBS) in the dark for 30 min at ambient temperature followed by FACSCalibur analysis.

2.6.4. Transwell Assay. Cell invasion ability was measured using the transwell assay. In detail, HepG2 cells (4×10^5 cells) were seeded in a 6-well plate and pretreated with MSN-PEG, free-TanIIA, MSN-TanIIA, and MSN-TanIIA-PEG.

Initially, 50 mg/L Matrigel (BD Biosciences, USA) was coated onto the transwell insert membrane at a 1 : 8 dilution at the apical side. After collection from every group, the cells were resuspended in a serum-free medium, and then 1×10^5 cells (200 μL) were transferred into the upper transwell chambers (8 μm ; BD Biosciences, USA). The inferior chamber was filled with 500 μL of 10% FBS-containing DMEM. Following 24-h incubation at 37°C, the cells were subjected to twice PBS washing, 30-min fixation in 4% paraformaldehyde, and 20-min staining with crystal violet (0.1%) at room temperature. Then, the cells were washed with water 3 times. After this, a cotton swab was used to remove the nontraveled cells from the upper filter surface in a gentle manner. Finally, the cell pictures were obtained under a microscope and the cell numbers were quantified with ImageJ software. The cell invasion inhibition rate was calculated following this formula: The cell invasion inhibition rate (%) = $(\text{cells' count of untreated group} - \text{cells' count of the treatment group}) / \text{cells' count of untreated group} \times 100$.

2.7. Construction and Identification of the GPC3-shRNA Plasmid. The GPC3-shRNA plasmid was constructed as our previous description [25]. The plasmid was purchased from Manfute biotech (Nanjing, China). Human GPC3 sequences (GenBank ID: 2719) were selected as the target site for RNAi. For pSLenti-GPC3-shRNA plasmid construction, driven by the U6 promoter, the annealed oligonucleotides (double-stranded) were inserted into pSLenti plasmids by T4 DNA ligation using AegI-EcoRI restriction sites. The primer sequence (designed by Primer3 software) upstream was 5'-CCGGCCGAAGAAGGGAAGCTAATTCTCAAGAGAAA-TTAGTTCCTTCTTCGGTTTTTTG-3', and the downstream was 5'-AATTCAAAAACCGAAGAAGGGAAGCTAATTCTCTTGAGAATTAGTTCCTTCTTCGG-3'. After shaking the bacterial solution, the positive clones were identified by PCR, the reaction conditions of GPC3-

shRNA were as follows: initial denaturation at 95°C for 5 min; 30 cycles of 94°C for 30 s, 60°C for 30 s, and extension at 72°C for 60 s, followed by the final extension at 72°C for 10 min. Finally, sequence verification of the resulting pSLenti-U6-GPC3-shRNA plasmids was accomplished via DNA sequencing. Then, the vector NTI software was used to compare and analyze the sequencing results. Meanwhile, to examine the transfection efficiency, GPC3-shRNA-EGFP plasmids were constructed as well.

2.8. DNA Binding, Digestion Protection, and Release Experiments. For DNA binding, digestion protection, and release experiments, the methods reported in our previous work were used and the methods description partly reproduced our earlier wording [25].

2.8.1. MSN-PEG Binding with GPC3-shRNA Experiment. To obtain the proper mass ratio of GPC3-shRNA plasmids to MSN-PEG, the same amount of shRNA was incubated with different concentrations of MSN-PEG solutions. GPC3-shRNA plasmids and MSN-PEG were mixed at the mass ratios of 1:0 (naked shRNA), 1:5, 1:10, 1:20, 1:40, 1:60, 1:80, and 1:100 (final plasmid concentration: 20 ng/ μ L). After 60 min of incubation at room temperature, 5 μ L of each MSN/shRNA complex was subjected to 1% agarose gel electrophoresis (AGE) using 0.5 μ g/mL ethidium bromide (EB), with 40-min running of the gels at 110 V with Tris-acetate (TAE) buffer. Retardation of the motion of shRNA was observed with a UV lamp by using a G:BOX Chemi XX9 imaging system (Syngene, UK).

2.8.2. DNA Digestion Protection Capacity. GPC3-shRNA plasmids and MSN-PEG were mixed to form a complex according to a mass ratio of 1:20. The complex was then digested with DNase-I enzyme and Tango Buffer at 37°C for 1, 10, 30, 45, and 60 min. Later, the reaction was terminated by adding EDTA solution (100 mmol/L). This was followed by washing, drying of resultants, and a subsequent dissolution in 200 μ L ultrapure water. The naked shRNA plasmid DNA (pDNA) was treated the same way and served as a control. Finally, 5 μ L of each product was electrophoresed.

2.8.3. DNA Release Capacity of the Complex. GPC3-shRNA plasmids (10 μ g) and MSN-PEG were mixed to form a complex according to a mass ratio of 1:20. The complex was made to a 500 μ L volume by mixing with TE solution. For AGE detection, 5 μ L of sample was taken separately at 1, 4, 8, 12, 24, 48, 72, and 96 h.

2.9. MSN-PEG Transfection Efficiency Detection. MSN-PEG and GPC3-shRNA-EGFP plasmids were individually dispersed in the DMEM culture medium. MSN-PEG and GPC3-shRNA-EGFP plasmids were incubated at a mass ratio of 20:1 for 30 min to make them mix sufficiently.

After HepG2 cells were cultured overnight, the medium was replaced with the above mixture. The culture medium was replaced by fresh DMEM after 5-h incubation. Additional 24-h incubation sustained before harvesting cells. Meanwhile, Lipofectamine 2000 transfection method, which conducted according to the instruction, served as comparison. The two methods' transfection efficiencies were observed using a fluorescence microscope and analyzed via FACSCalibur.

2.10. Quantitative Real-Time Polymerase Chain Reaction (PCR) Analysis. Using MSN-PEG as a carrier, the GPC3-shRNA plasmids and negative control were transfected into the HepG2 cells, and 24 h later, cellular mRNA detection of GPC3 was carried out by qRT-PCR. TRIzol reagent (Invitrogen, USA) was used to extract the cellular total RNA as per the instructions of the manufacturer. One microgram of RNA was reverse transcribed into cDNA using ReverTra Ace™ qPCR RT Master Mix (TOYOBO Biotech, Japan). The reaction solution was subjected to 15-min incubation at 37°C and a subsequent 5-min heating to 98°C as per the instructions of the manufacturer. The final step was qRT-PCR analysis on an Applied Biosystems 7500 Real-Time PCR instrument (Thermo Fisher, USA). The comparative Ct ($2^{-\Delta\Delta C_t}$) method was used to calculate the relative fold changes of mRNA expression in different groups. The primer sequences are as follows: GPC3 (Beyotime, China): 5'-CCTTTGAAATTGTTGCGCA-3' (forward) and 5'-CCTGGGTTTCATTAGCTGGGTA-3' (reverse); GAPDH (Beyotime, China): 5'-CATCTTCTTTGCGTCGCCA-3' (forward) and 5'-TTAAAA-GCAGCCCTGGTGACC-3' (reverse).

2.11. Western Blotting. Total proteins from transfected and untransfected HepG2 cells were extracted using RIPA buffer (Vazyme Biotech, China). BCA assay (Beyotime, China) was conducted to quantify the extracted total proteins. For isolation of the protein samples, 12% sodium dodecyl sulfate polyacrylamide gel electrophoresis (SDS-PAGE) was carried out followed by transfer to polyvinylidene fluoride membranes (0.45 μ m) with 300 mA current for 90 min. After transfer, the membranes were blocked in 5% BSA at ambient temperature for 1 h and then incubated overnight using rabbit antibodies against GPC3 (Abcam, USA; diluted 1:1000) and a rabbit antibody against GAPDH (Sangon Biotech, China; diluted 1:5000) as an internal standard at 4°C to normalize the protein expressions. On the next day, the membranes were further incubated using goat anti-rabbit IgG-HRP (Sangon Biotech, China; diluted 1:5000) for 1 h and then subjected to protein visualization using enhanced chemiluminescence (Vazyme Biotech, China). The G:BOX Chemi XX9 imaging system (Syngene, UK) was used for protein visualization.

2.12. Statistical Analysis. Quantitative variables were represented as the mean \pm standard deviation ($\bar{x} \pm s$). $P < 0.05$ was considered statistically significant. The data were

determined by one-way ANOVA analysis using GraphPad Prism 8.0 software.

3. Results and Discussion

3.1. Characterization of Nanoparticles

3.1.1. Particle Size, Zeta Potential, and Morphological Features. It was reported that nanocarriers have high drug loading capacity, excellent tolerability, high stability, and low drug degradation, which achieve controlled release and sustained delivery of antineoplastics [26]. In this study, TanIIA-loaded MSN-PEG nanoparticles were prepared, as described previously. The DL and EE of MSN-TanIIA-PEG nanoparticles were 9.32% and 93.13%, respectively.

Figures 2(a)–2(h) display the size distribution of the particles, as well as the zeta potential of the MSN, MSN-TanIIA, MSN-TanIIA-PEG, and MSN-PEG. As suggested by the results of DLS assessment, MSN has a hydrodynamic size of 78 nm and a zeta potential of -36.0 mV. With the gradual modification of the MSN nanoparticles with TanIIA and PEI-PEG, the MSN-TanIIA and MSN-TanIIA-PEG exhibited increases in the hydrodynamic size separately to 90 nm and 117 nm. Besides, the surface charges of MSN and MSN-TanIIA were -36 mV and -30 mV, indicating negative charges. Interestingly, both MSN-TanIIA-PEG and MSN-PEG had positive charges with values of 43.2 mV and 47 mV, respectively. This verified the negative-to-positive changes in the surface charges of nanoparticles. The foregoing results imply the successful modification of nanoparticles. Moreover, the positive charges enabled formation of an electrostatic complex by the carrier with shRNA, thereby protecting it from nucleases and facilitating its cellular uptake [27].

TEM analysis was performed to elucidate the morphology of the nanoparticles. According to the TEM micrographs in Figures 2(i)–2(l), the majority of the nanoparticles, regardless of modified or not, was about 50 nm in particle size, which had a regular spherical shape, uniform particle size, and good monodispersity. The surface-modified particles maintained the basic morphology. Additionally, it was obviously observed that the surface mesoporous pores became blurred, and there was a white halo on the nanoparticle periphery, which corresponded to the surface modification with the polymer layer. It has been reported that nanoparticles with a size of 100–200 nm can be quickly eliminated from the blood by macrophages in the RES after entering the circulation. In contrast, the nanoparticles 50–100 nm in size are capable of entering liver cells and target drugs to the liver [2]. According to the EPR effect, nanoparticles with particle size less than 100 nm can easily pass through the interstices of the tumor tissue and thus remain in the tumor tissue [28]. In the present study, the prepared nanoparticle size was about 50 nm, which is in accordance with the preparation requirements of particle size between 50 nm and 100 nm.

3.1.2. In Vitro Drug Release. Some studies have demonstrated that the entrapped drug release from the

nanoparticles in a sustained manner extended the plasma biological half-life for the natural compounds [29, 30]. For effectiveness validation of the nanoparticles in drug delivery, the *in vitro* release of TanIIA from MSN-TanIIA and MSN-TanIIA-PEG was employed at various time intervals (1, 2, 4, 6, 8, 12, 18, and 24 h), and the curve of TanIIA release was plotted (Figure 2(m)). According to the *in vitro* TanIIA release curve, both MSN-TanIIA and MSN-TanIIA-PEG showed a typical pattern of two-phase release. The TanIIA from MSN-TanIIA and MSN-TanIIA-PEG was initially released at a rapid rate with 71.89% and 59.7% in the first 6 h, which was denoted as incubation period. From 7 to 24 h, the sustained release phase, the cumulative release of the drug gradually increased. After 12 h, the release gradually decreased, which was followed by the smooth release until 24 h. The sustained release reached 97.27% and 97.95% at 24 h for MSN-TanIIA and MSN-TanIIA-PEG, respectively. It was obviously seen that the percentage of TanIIA release in MSN-TanIIA was higher than that of MSN-TanIIA-PEG. The high burst release of MSN-TanIIA may prevent drugs from reaching to the target tissues or cells, thus making it less effective. On the contrary, the sustained release of MSN-TanIIA-PEG was more suitable for the drug release properties of nanoparticles [31].

3.2. In Vitro Antitumor Activity

3.2.1. Cell Proliferation Inhibition Assay. The cell growth inhibition effect was examined under various concentrations of free-TanIIA, MSN-TanIIA, and MSN-TanIIA-PEG (0–80 $\mu\text{g}/\text{mL}$) using the CCK-8 kit. The results revealed increases in the growth inhibition rates of HepG2 cells in a dose-dependent manner. The IC_{50} of free-TanIIA, MSN-TanIIA, and MSN-TanIIA-PEG were 14.842 $\mu\text{g}/\text{mL}$, 9.298 $\mu\text{g}/\text{mL}$, and 6.959 $\mu\text{g}/\text{mL}$, respectively (Figure 3(a)), while the blank nanoparticles (MSN-PEG) and DMSO had no significant effects on the cells' growth. Suggestively, the slower and sustained TanIIA release from the MSN-TanIIA-PEG led to reduced effective dose (IC_{50}) and obtained superior therapeutic efficacy *in vitro* to the free-TanIIA for HCC cells. Similar observations have also been reported by Yang et al. [12] and Sun et al. [21], where IC_{50} of many nanoparticles of natural products was lower than that of the free products.

3.2.2. Cell Apoptosis Assays. Hoechst 33342 is typically used for detecting cell apoptosis, and the principle is that it can permeate apoptotic cellular membranes freely, and that apoptotic cells can be identified by the bright blue-stained nuclei that are either condensed or scattered [32]. The apoptotic cell nuclei exhibit a high intensity of fluorescence, while weak fluorescence is noted in the nonapoptotic cells [33]. To evaluate the apoptosis of HepG2 cells induced by MSN-PEG, free-TanIIA, MSN-TanIIA, and MSN-TanIIA-PEG, the cellular nuclei were stained using Hoechst 33342 followed by fluorescence microscope evaluation. Compared

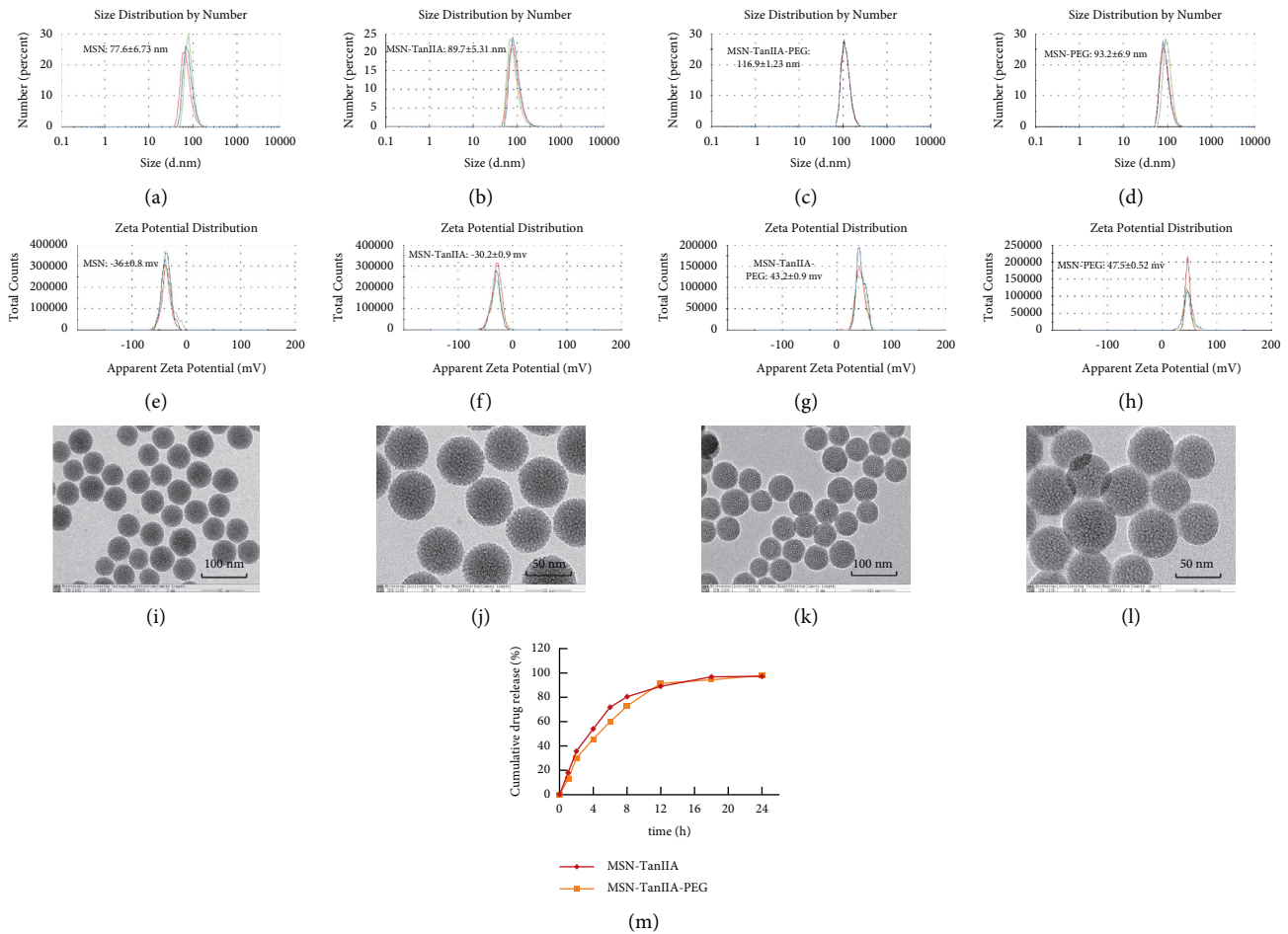


FIGURE 2: Characterization of nanoparticles. (a–d) The size distribution of nanoparticles. (e–h) The zeta potential of nanoparticles. (i–l) Nanoparticle morphological features were analyzed with TEM at different magnification ratios. (i, j) MSN. (k, l) MSN-TanIIA-PEG. (m) Cumulative drug release curve *in vitro*.

with the intact control nuclei, the cells intervened with MSN-PEG showed little difference, while the cells intervened with free-TanIIA, MSN-TanIIA, and MSN-TanIIA-PEG all exhibited nucleus shrinkage and were stained bright blue or showed debris-like lobulation of nuclei (Figure 3(b)). However, within similar sized fields, there were more apoptotic cells in the MSN-TanIIA-PEG group than in the free-TanIIA and MSN-TanIIA groups. This observation is consistent with a previous finding that noisome-coated TanIIA could enhance the apoptosis of HepG2 cells [2].

Subsequently, HepG2 cells intervened with MSN and TanIIA were doubly stained with Annexin V-Alexa Fluor 647 plus PI, and then the cell apoptosis induced by intervention was determined by flow cytometry. As shown in Figure 3(c), the control cells exhibited an exceptionally low apoptosis rate, which was only $8.26 \pm 2.83\%$. In contrast, the cell apoptosis induced by MSN-PEG, free-TanIIA, MSN-TanIIA, and MSN-TanIIA-PEG amounted to $12.81 \pm 3.40\%$, $18.92 \pm 3.55\%$, $30.63 \pm 4.09\%$, and $38.68 \pm 6.57\%$, respectively. Obviously, the cell apoptosis induced by MSN-TanIIA-PEG was far stronger than that induced by other methods ($P < 0.05$). The finding was consistent with the

result of Hoechst 33342 staining assay. Moreover, the apoptotic results coincided with the cell proliferation inhibition data as well.

3.2.3. Cell Cycle Assay. Following the verification of cell apoptosis effect induced by MSN-TanIIA-PEG, flow cytometry was utilized to analyze the variation trends of HepG2 cell distribution by the MSN-PEG, free-TanIIA, MSN-TanIIA, and MSN-TanIIA-PEG over the cell cycle phases. According to Figure 3(d), the MSN-TanIIA-PEG intervention group showed an increased G0/G1 phase cell population compared with the control group, which was also more significant than the MSN-PEG, free-TanIIA, and MSN-TanIIA intervention groups. This finding suggested that nano-TanIIA intervention could affect the arrest of cell cycle at G0/G1, the phases of DNA replication [34]. In other words, MSN-TanIIA-PEG prevented the duplication of DNA, diminished the S phase cell proportion during DNA synthesis, and inhibited the G2/M phase accumulation of cells. As a result, HepG2 cells' growth and proliferation were effectively suppressed.

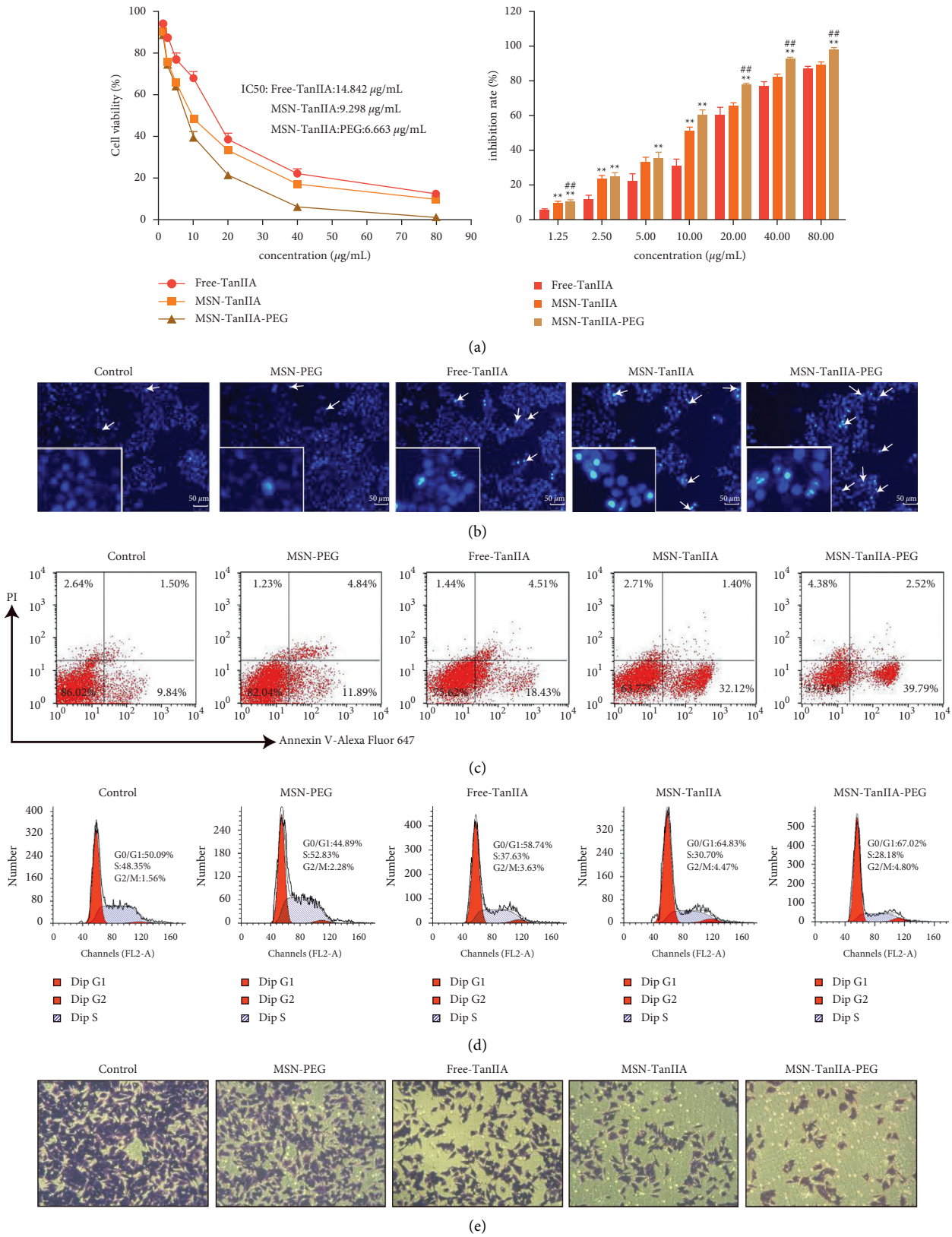


FIGURE 3: *In vitro* antitumor activity of MSN-TanIIA-PEG. (a) Inhibition rate of HepG2 cells under free-TanIIA, MSN-TanIIA, and MSN-TanIIA-PEG treatment for 24 h (** $P < 0.05$ vs. the control group and $###P < 0.05$ vs. other counterparts). (b) Hoechst staining of HepG2 cells incubated with MSN-PEG, free-TanIIA, MSN-TanIIA, and MSN-TanIIA-PEG for 24 h. (c) Apoptosis of HepG2 cells intervened with MSN-PEG, free-TanIIA, MSN-TanIIA, and MSN-TanIIA-PEG for 24 h. (d) Cell cycle distribution of HepG2 cells in different groups. (e) Results of the HepG2 cells' invasion experiment in different experimental groups.

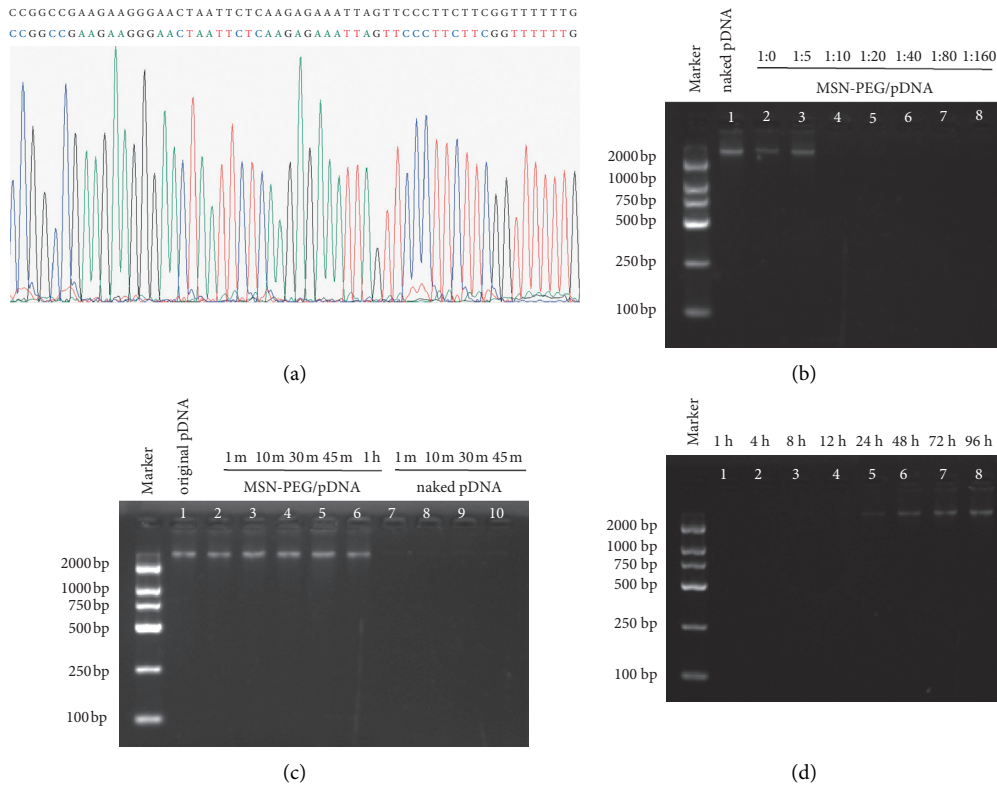


FIGURE 4: Identification of GPC3-shRNA plasmids and MSN-PEG. (a) GPC3-shRNA sequencing comparison results. (b–d). Binding, digestion, and release of MSN-PEG with GPC3-shRNA plasmid. (b) Electrophoresis image of MSN-PEG with various mass ratios after binding with GPC3-shRNA plasmids. (c) Electrophoresis image of the release experiment of MSN-PEG/GPC3-shRNA complex. (d) Electrophoresis image of the digestion protection experiment of MSN-PEG/GPC3-shRNA complex.

This finding is consistent with the previous research showing the ability of TanIIA to arrest cells at the *G0/G1* checkpoint in a dose-related manner [35, 36]. It also agreed with the finding of another study demonstrating a differing effect of the drug-entrapped nanoparticles on the distribution of cell cycle from the free-form drug [37]. However, the effect of TanIIA on the cell cycle distribution remains controversial. Some studies observed that TanIIA could arrest cells at the *S/G2* phases [37, 38]. After HepG2 cells were intervened with MSN-TanIIA-PEG, the *G0/G1* phase cell distribution increased, while the proportion of *S* and *G2/M* phase cells decreased, which remains to be further explored.

3.2.4. Cell Invasion Ability Assay. To explore the role of TanIIA in the HCC development, the transwell experiment was employed to examine how TanIIA affected the HepG2 cell invasiveness. Similar to the above outcomes, TanIIA showed remarkable suppression of cell invasion. The cell invasion inhibition rate of the free-TanIIA group was $35.95 \pm 8.98\%$, which was higher than MSN-PEG group's $20.17 \pm 8.54\%$ (Figure 3(e)). Compared with the free-TanIIA group, the cell invasion inhibition rate in nano-TanIIA groups (MSN-TanIIA: $59.66 \pm 5.09\%$ and MSN-TanIIA-PEG: $71.61 \pm 2.58\%$) was significantly increased. As shown in Figure 3(e), HepG2 cells intervened with MSN-TanIIA-PEG

exhibited higher cell invasion inhibition rates than other counterparts. These results indicated that MSN-TanIIA-PEG has the strongest cell invasion inhibition effect on HepG2 cells.

Taken together, our findings suggested that MSN-TanIIA-PEG could suppress HCC cell growth and invasion and promote apoptosis, which may exert a crucial effect on the HCC progression. However, the specific mechanism still needs further verification by molecular biology experiments.

3.3. Identification of GPC3-shRNA Plasmid. The presence of correct clones was identified by sequencing comparison, which implied that the GPC3-shRNA plasmids were constructed successfully (Figure 4(a)).

3.4. Binding, Release, and Digestion of MSN-PEG with GPC3-shRNA Plasmids. Gene therapy targeting GPC3 holds a tremendous potential for HCC treatment, especially the RNAi therapy. The primary difficulty in its clinical application is still the safe and efficient design of delivery carriers. Inspiringly, PEG, a neutral and hydrophilic polymer, has been used widely, which helped lower the cytotoxicity and extend the circulation time. Moreover, there has also been a broad application of positively charged PEI owing to its high DNA condensing and transfection efficiencies [20, 39]. The ability of plasmid binding onto MSN-PEG and the capacities

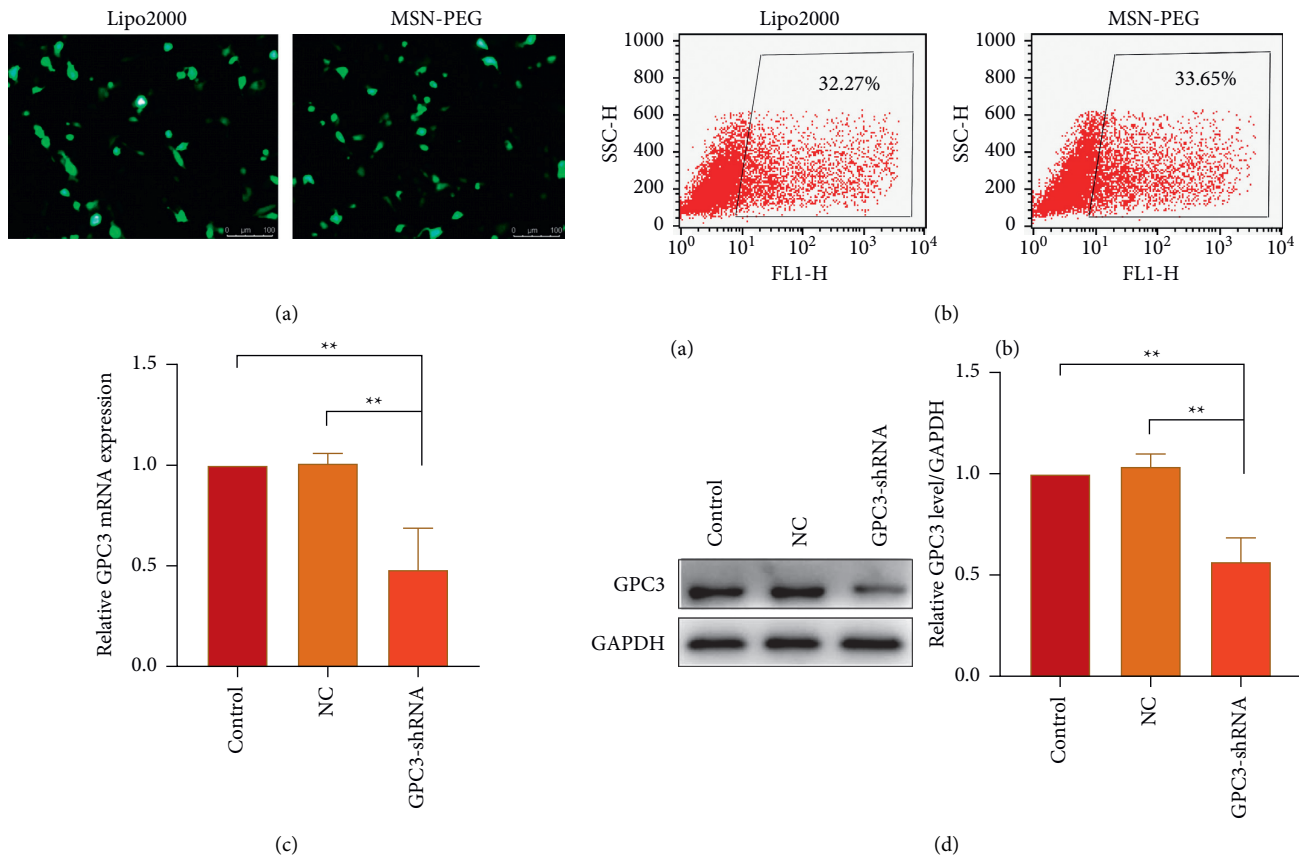


FIGURE 5: Evaluation of MSN-PEG gene transfection efficiency. (a) The transfection efficiency observed using a fluorescence microscope. (b) The transfection efficiency detected by flow cytometry. (c) GPC3 mRNA expression of transfected HepG2 cells detected by quantitative real-time PCR. (d) GPC3 protein expression of transfected HepG2 cells examined by Western blotting ((a) Protein bands. (b) Quantitative statistical results according to the protein bands). (** $P < 0.05$ vs. the transfected with negative control plasmid group and untransfected group).

of DNA digestion protection and release were identified by gel retardation assays. As seen from electrophoresis image, when plasmids were added at mass ratios (GPC3-shRNA to MSN-PEG) of 1:0, 1:5, and 1:10, a clear band was observable in the corresponding lane. When the mass ratio was 1:20, no band could be observed (Figure 4(b)), indicating that GPC3-shRNA plasmids could be completely loaded onto the nanoparticles, so that the optimal binding ratio was 1:20.

Electrophoresis of release assay revealed that no DNA band was observed at 1, 4, 8, 12, or 24 h. Nevertheless, the brightness of the electrophoretic band increased within 48 and 72 h, and there was no significant difference between the 3rd and the 4th day, indicating that MSN-PEG was capable of protecting the pDNA from degradation and reasonably releasing pDNA under appropriate conditions (Figure 4(c)).

In order to observe the stability of the nanoparticle/pDNA complex, the DNase-I digestion experiment was performed. After the complex of MSN-PEG/GPC3-shRNA was added with DNase-I enzyme, the brightness of the electrophoretic band remained stable in the first 1 h. On the contrary, after digestion with DNase-I enzyme, the naked pDNA was almost completely digested within 1 min, and no

bands could be seen on the electrophoresis lane, verifying that nanoparticles could effectively protect the pDNA from nuclease digestion (Figure 4(d)).

3.5. Evaluation of MSN-PEG Gene Transfection Efficiency. Using MSN-PEG as a carrier, the GPC3-shRNA-EGFP plasmids were transfected into HepG2 cells for the transfection efficiency observation of GPC3-shRNA plasmids under a fluorescence microscope. As the EGFP expression indicated, no obvious difference was observed in transfection efficiency between MSN-PEG and Lipo2000 in the HepG2 cells (Figure 5(a)). Besides, the transfection efficiency of MSN-PEG was $34.37 \pm 1.06\%$ as analyzed by flow cytometry, with no significant difference from the liposome group's $31.78 \pm 1.30\%$ (Figure 5(b)). As suggested by the foregoing findings, MSN-PEG has an encouraging potential as a gene-transferring carrier in gene therapy.

HepG2 cells were transfected with GPC3-shRNA via MSN-PEG for 24 h, and then GPC3 gene expression was examined by qRT-PCR combined with Western blotting. It was found that GPC3 mRNA expression in the untransfected (control) group differed indistinctly from that in the

negative control (NC) group, although they were both higher than that in the GPC3-shRNA plasmid-transfected group (Figure 5(c)). Correspondingly, the expression level of GPC3 protein was reduced after GPC3-shRNA plasmid transfection, as shown in Figure 5(d). This further confirms the successful establishment of GPC3-shRNA plasmids and the workability of using MSN-PEG to transfer target gene in gene therapy. In a word, it offered a new idea of using MSN-PEG as a vector to carry TanIIA and GPC3-shRNA for comprehensive treatment of HCC in clinics.

4. Conclusion

In this study, MSN-TanIIA-PEG with favorable dispersity and biological characteristics was successfully prepared. The anti-tumor efficacies of nano-TanIIA on HCC *in vitro* were greatly improved, which outperformed free-TanIIA in terms of proliferation and invasion inhibition, and apoptosis induction of HCC cells. Capable of releasing TanIIA into carcinoma cells in a sustained manner, this formulation may be an appropriate candidate for pharmacological application. Nonetheless, the specific mechanism still needs to be further explored, and its efficacy and safety deserve more *in vivo* investigations before clinical trials. Additionally, GPC3-shRNA plasmids were successfully constructed, and MSN-PEG showed an excellent gene transfection efficiency and may thus serve as a carrier for gene therapy. The findings of this study also offer a novel idea for HCC treatment, where MSN-PEG is used as a carrier to combine TanIIA together with GPC3-shRNA.

Data Availability

The graphics and quantitative data used to support the findings of this study are included within the article.

Conflicts of Interest

The authors declare that they have no conflicts of interest.

Acknowledgments

This work was supported by the National Natural Science Foundation of China (81571797), the Social Development Plan of Taizhou, China (TS202004), the Natural Science Foundation of Nanjing University of Chinese Medicine, China, (XZR2020093), and Taizhou People's Hospital Medical Innovation Team Foundation, China (CXTDA201901).

References

- [1] H. Sung, J. Ferlay, R. L. Siegel et al., "Global cancer statistics 2020: GLOBOCAN estimates of incidence and mortality worldwide for 36 cancers in 185 countries," *CA: A Cancer Journal for Clinicians*, vol. 71, no. 3, pp. 209–249, 2021.
- [2] X. Hu, J. Zhang, L. Deng, H. Hu, J. Hu, and G. Zheng, "Galactose-modified PH-sensitive niosomes for controlled release and hepatocellular carcinoma target delivery of tanshinone IIA," *AAPS PharmSciTech*, vol. 22, no. 3, p. 96, 2021.
- [3] L. Li, X. Zhang, C. Pi et al., "Review of curcumin physico-chemical targeting delivery system," *International Journal of Nanomedicine*, vol. 15, pp. 9799–9821, 2020.
- [4] X. Wang, S. L. Morris-Natschke, and K.-H. Lee, "New developments in the chemistry and biology of the bioactive constituents of Tanshen," *Medicinal Research Reviews*, vol. 27, no. 1, pp. 133–148, 2007.
- [5] Z. Y. Fang, M. Zhang, J. N. Liu, X. Zhao, Y. Q. Zhang, and L. Fang, "Tanshinone IIA: a review of its anticancer effects," *Frontiers in Pharmacology*, vol. 11, Article ID 611087, 2020.
- [6] M. A. Ansari, F. B. Khan, H. A. Safdari et al., "Prospective therapeutic potential of Tanshinone IIA: an updated overview," *Pharmacological Research*, vol. 164, Article ID 105364, 2021.
- [7] Z.-Y. Zhou, W.-R. Zhao, J. Zhang, X.-L. Chen, and J.-Y. Tang, "Sodium tanshinone IIA sulfonate: a review of pharmacological activity and pharmacokinetics," *Biomedicine & Pharmacotherapy*, vol. 118, Article ID 109362, 2019.
- [8] H.-m. Yan, E. Sun, L. Cui, X.-b. Jia, and X. Jin, "Improvement in oral bioavailability and dissolution of tanshinone IIA by preparation of solid dispersions with porous silica," *Journal of Pharmacy and Pharmacology*, vol. 67, no. 9, pp. 1207–1214, 2015.
- [9] Z. Li, Y. Zhang, K. Zhang, Z. Wu, and N. Feng, "Biotinylated-lipid bilayer coated mesoporous silica nanoparticles for improving the bioavailability and anti-leukaemia activity of Tanshinone IIA," *Artificial Cells, Nanomedicine, and Biotechnology*, vol. 46, no. sup1, pp. 578–587, 2018.
- [10] T. Moodley and M. Singh, "Sterically stabilised polymeric mesoporous silica nanoparticles improve doxorubicin efficiency: tailored cancer therapy," *Molecules*, vol. 25, no. 3, 2020.
- [11] Y. Tang, X. Wang, J. Li et al., "Overcoming the reticuloendothelial system barrier to drug delivery with a "Don't-Eat-Us" strategy," *ACS Nano*, vol. 13, no. 11, pp. 13015–13026, 2019.
- [12] S. Yang, Z. Wang, Y. Ping et al., "PEG/PEI-functionalized single-walled carbon nanotubes as delivery carriers for doxorubicin: synthesis, characterization, and *in vitro* evaluation," *Beilstein Journal of Nanotechnology*, vol. 11, pp. 1728–1741, 2020.
- [13] F. Zhou, W. Shang, X. Yu, and J. Tian, "Glypican-3: a promising biomarker for hepatocellular carcinoma diagnosis and treatment," *Medicinal Research Reviews*, vol. 38, no. 2, pp. 741–767, 2018.
- [14] T.-C. Shih, L. Wang, H.-C. Wang, and Y.-J. Y. Wan, "Glypican-3: a molecular marker for the detection and treatment of hepatocellular carcinoma," *Liver Research*, vol. 4, no. 4, pp. 168–172, 2020.
- [15] M. Mroweh, T. Decaens, P. N. Marche, Z. Macek Jilkova, and F. Clément, "Modulating the crosstalk between the tumor and its microenvironment using RNA interference: a treatment strategy for hepatocellular carcinoma," *International Journal of Molecular Sciences*, vol. 21, no. 15, 2020.
- [16] R. Acharya, "Prospective vaccination of COVID-19 using shRNA-plasmid-LDH nanoconjugate," *Medical Hypotheses*, vol. 143, p. 110084, 2020.
- [17] G. Tian, R. Pan, B. Zhang et al., "Liver-targeted combination therapy basing on glycyrrhizic acid-modified DSPE-PEG-PEI nanoparticles for Co-delivery of doxorubicin and bcl-2 siRNA," *Frontiers in Pharmacology*, vol. 10, p. 4, 2019.
- [18] Y. Gu, Y. Guo, C. Wang et al., "A polyamidoamine dendrimer functionalized graphene oxide for DOX and MMP-9 shRNA

- plasmid co-delivery," *Materials Science and Engineering: C*, vol. 70, no. 1, pp. 572–585, 2017.
- [19] X. Guo, Z. Yuan, Y. Xu, M. Wei, Z. Fang, and W.-E. Yuan, "A fluorinated low-molecular-weight PEI/HIF-1 α shRNA polyplex system for hemangioma therapy," *Biomaterials Science*, vol. 8, no. 8, pp. 2129–2142, 2020.
- [20] M. Zhao, J. Li, H. Ji, D. Chen, and H. Hu, "A versatile endosome acidity-induced sheddable gene delivery system: increased tumor targeting and enhanced transfection efficiency," *International Journal of Nanomedicine*, vol. 14, pp. 6519–6538, 2019.
- [21] Z. Li, Y. Zhang, C. Zhu et al., "Folic acid modified lipid-bilayer coated mesoporous silica nanoparticles co-loading paclitaxel and tanshinone IIA for the treatment of acute promyelocytic leukemia," *International Journal of Pharmaceutics*, vol. 586, Article ID 119576, 2020.
- [22] X. Liu and X. Chen, "Determination of tanshinone IIA in radix salviae miltiorrhizae by HPLC," *Fujian Analysis and Testing*, vol. 24, no. 1, pp. 36–38, 2015.
- [23] Y. Amini, S. Amel Jamehdar, K. Sadri, S. Zare, D. Musavi, and M. Tafaghodi, "Different methods to determine the encapsulation efficiency of protein in PLGA nanoparticles," *Bio-Medical Materials and Engineering*, vol. 28, no. 6, pp. 613–620, 2017.
- [24] Y. Salinas, O. Brüggemann, U. Monkowius, and I. Teasdale, "Visible light photocleavable ruthenium-based molecular gates to reversibly control release from mesoporous silica nanoparticles," *Nanomaterials*, vol. 10, no. 6, 2020.
- [25] T. Guo, F. Dou, M. Lin et al., "Biological characteristics and carrier functions of pegylated manganese zinc ferrite nanoparticles," *Journal of Nanomaterials*, vol. 2019, pp. 1–10, 2019.
- [26] U. Ruman, S. Fakurazi, M. J. Masarudin, and M. Z. Hussein, "Nanocarrier-based therapeutics and theranostics drug delivery systems for next generation of liver cancer nanodrug modalities," *International Journal of Nanomedicine*, vol. 15, pp. 1437–1456, 2020.
- [27] J. Yu, J. Zhang, H. Xing et al., "Novel guanidinylated bio-responsive poly(amidoamine)s designed for short hairpin RNA delivery," *International Journal of Nanomedicine*, vol. 11, pp. 6651–6666, 2016.
- [28] D.-H. Park, J. Cho, O.-J. Kwon, C.-O. Yun, and J.-H. Choy, "Biodegradable inorganic nanovector: passive versus active tumor targeting in siRNA transportation," *Angewandte Chemie International Edition*, vol. 55, no. 14, pp. 4582–4586, 2016.
- [29] H.-Y. Zhang, C.-y. Sun, M. Adu-Frimpong, J.-n. Yu, and X.-m. Xu, "Glutathione-sensitive PEGylated curcumin pro-drug nanomicelles: preparation, characterization, cellular uptake and bioavailability evaluation," *International Journal of Pharmaceutics*, vol. 555, pp. 270–279, 2019.
- [30] C. Ceci, G. Graziani, I. Faraoni, and I. Cacciotti, "Strategies to improve ellagic acid bioavailability: from natural or semi-synthetic derivatives to nanotechnological approaches based on innovative carriers," *Nanotechnology*, vol. 31, no. 38, p. 382001, 2020.
- [31] A. Iadnut, K. Mamoon, P. Thammasit et al., "In vitro antifungal and antivirulence activities of biologically synthesized ethanolic extract of propolis-loaded PLGA nanoparticles against *Candida albicans*," *Evid Based Complement Alternat Med*, vol. 2019, Article ID 3715481, 14 pages, 2019.
- [32] Y. Liu, J. Zheng, Y. Zhang et al., "Fucoxanthin activates apoptosis via inhibition of PI3K/Akt/mTOR pathway and suppresses invasion and migration by restriction of p38-MMP-2/9 pathway in human glioblastoma cells," *Neurochemical Research*, vol. 41, no. 10, pp. 2728–2751, 2016.
- [33] F. Teng, Z. Xu, J. Chen et al., "DUSP1 induces apatinib resistance by activating the MAPK pathway in gastric cancer," *Oncology Reports*, vol. 40, no. 3, pp. 1203–1222, 2018.
- [34] W. Sun, Y. Wang, M. Cai et al., "Codelivery of sorafenib and GPC3 siRNA with PEI-modified liposomes for hepatoma therapy," *Biomaterials Science*, vol. 5, no. 12, pp. 2468–2479, 2017.
- [35] C.-Y. Huang, T.-L. Chiu, S.-J. Kuo, S.-Y. Chien, D.-R. Chen, and C.-C. Su, "Tanshinone IIA inhibits the growth of pancreatic cancer BxPC-3 cells by decreasing protein expression of TCTP, MCL-1 and Bcl-xL," *Molecular Medicine Reports*, vol. 7, no. 3, pp. 1045–1049, 2013.
- [36] X. Ren, C. Wang, B. Xie et al., "Tanshinone IIA induced cell death via miR30b-p53-PTPN11/SHP2 signaling pathway in human hepatocellular carcinoma cells," *European Journal of Pharmacology*, vol. 796, pp. 233–241, 2017.
- [37] F. Chen, J. Zhang, Y. He, X. Fang, Y. Wang, and M. Chen, "Glycyrrhetic acid-decorated and reduction-sensitive micelles to enhance the bioavailability and anti-hepatocellular carcinoma efficacy of tanshinone IIA," *Biomaterials Science*, vol. 4, no. 1, pp. 167–182, 2016.
- [38] X. Liao, Y. Gao, J. Liu et al., "Combination of tanshinone IIA and cisplatin inhibits esophageal cancer by downregulating NF- κ B/COX-2/VEGF pathway," *Frontiers in Oncology*, vol. 10, p. 1756, 2020.
- [39] B. Saqafi and F. Rahbarizadeh, "Polyethyleneimine-polyethylene glycol copolymer targeted by anti-HER2 nanobody for specific delivery of transcriptionally targeted tBid containing construct," *Artificial Cells, Nanomedicine, and Biotechnology*, vol. 47, no. 1, pp. 501–511, 2019.

Research Article

Microencapsulated Recombinant Human Epidermal Growth Factor Ameliorates Osteoarthritis in a Murine Model

Shih-Chao Lin ¹, Xiang Zhang,² Shio-Yi Chen ³, Chi-Chien Lin ⁴ and Yen-Shuo Chiu ^{5,6}

¹Bachelor Degree Program in Marine Biotechnology, College of Life Sciences, National Taiwan Ocean University, Keelung 20224, Taiwan

²Department of Physiology and Pharmacology, Karolinska Institute, Stockholm SE-171 77, Sweden

³Department of Bioscience and Biotechnology, National Taiwan Ocean University, Keelung City 20224, Taiwan

⁴Institute of Biomedical Sciences, National Chung Hsing University, Taichung 402, Taiwan

⁵Department of Orthopedics, Shuang Ho Hospital, New Taipei 235, Taiwan

⁶School of Nutrition and Health Sciences, College of Nutrition, Taipei Medical University, Taipei 110, Taiwan

Correspondence should be addressed to Chi-Chien Lin; lincc@email.nchu.edu.tw and Yen-Shuo Chiu; yschiu12369@yahoo.com.tw

Received 15 May 2021; Revised 17 August 2021; Accepted 1 September 2021; Published 23 September 2021

Academic Editor: Muhammad Taher

Copyright © 2021 Shih-Chao Lin et al. This is an open access article distributed under the Creative Commons Attribution License, which permits unrestricted use, distribution, and reproduction in any medium, provided the original work is properly cited.

Osteoarthritis, a highly age-related and chronic inflammatory disorder with cartilage loss, causes patients difficulty in movement; there is no efficient and sustainable remedy for osteoarthritis currently. Although hyaluronic acid (HA) and platelet-rich plasma (PRP) have been used to alleviate osteoarthritis, the effects could be short and multiple injections might be required. To address this issue, we exploited the property of chitosan to encapsulate recombinant human epidermal growth factor and obtained microencapsulated rhEGF (Me-rhEGF). In the current study, we induced the osteoarthritis-like symptoms with monosodium iodoacetate (MIA) in rats and investigated the therapeutic effects of Me-rhEGF. Following administration of HA/Me-rhEGF *in vivo*, we observed that the total Mankin scores, cartilage oligomeric protein, C-telopeptide of type II collagen, IL-1 β , IL-6, IL-17A, and TNF- α cytokines, nitric oxide, and prostaglandin E2 expressions were significantly inhibited. Our results also strongly indicate that individual use of HA or rhEGF slightly decreased the inflammation and restored the destructive joint structure, but was not as drastic as seen in the HA/Me-rhEGF. Moreover, HA/Me-rhEGF profoundly reduced cartilage destruction and proteoglycan loss and downregulated matrix metalloproteinase expressions. These findings reveal that the treatment of HA/Me-rhEGF could be more beneficial than the use of single HA or rhEGF in reliving osteoarthritis and demonstrate the therapeutic application of microencapsulation technology in difficult joint disorders. In essence, we believe that the Me-rhEGF could be promising for further research and development as a clinical treatment against osteoarthritis.

1. Introduction

Osteoarthritis (OA) is a chronic, inflammatory, and degenerative joint disease, resulting in progressive cartilage damage. OA ultimately leads to cartilage loss, osteophyte formation (bone spurs), and bone thickening which in turn results in remodeling of affected joints. OA is more likely associated with patients that are elderly or obese. Estimably, there could be as high as 10–20% of people aged over 65 afflicted by OA [1]. At the age of 65, proteolytic enzyme levels increase in joint

tissues, subsequently resulting in degradation of the structural proteins of cartilage. Examples of such structural proteins include type II collagen and cartilage oligomeric matrix protein (COMP). Excess body weight debilitates the strength of joints, exacerbating the inflammatory condition [2]. Patients with OA could present symptoms with pain and joint swelling in the spine, ankles, hips, or knees. The primary therapeutic approach to treat OA is almost exclusively through pain management via administration of nonsteroidal anti-inflammatory drugs (NSAIDs) or acetaminophen.

However, such therapy does not successfully improve the symptoms or slow the progression of the disease [3].

In response to the lack of effective treatment, new remedies have been investigated for administration to OA patients, such as hyaluronic acid (HA). In 1997, the US Food and Drug Administration approved the use of HA by intra-articular injection to treat OA patients [4]. HA is one of the major components of synovial fluid. Additional supplement of HA can increase viscoelasticity and reduce the friction in joint tissues, attributing to the alleviation of inflammatory condition. However, the effect of HA injection may only persist for a number of weeks [5]. While a study in 1970 indicated that removing the HA from synovial fluid barely affected the joint lubrication [6]; visco-supplement injection might still be beneficial to OA patients with mild anti-inflammatory and placebo effects [7]. However, viscosity added by HA solution would eventually decrease to the level where lubricating property was lost, akin to the viscosity of water [8, 9].

Injection of growth factors, particularly platelet-rich plasma (PRP), has then been widely investigated as an alternative treatment of OA. However, due to the non-standardized methods for PRP preparation and the various physiological conditions of individuals, such as comorbidities, age, and circulation, the effect of PRP is inconsistent and debatable. PRP contains multiple growth factors, including tissue growth factor- β (TGF- β), insulin-like growth factor-1 (IGF-1), platelet-derived growth factor (PDGF), vascular endothelial growth factor (VEGF), fibroblast growth factor (FGF), and hepatocyte growth factor (HGF) in addition to various cytokines, chemokines, and coagulation factors [10].

Among these growth factors, ligands of EGF receptor (EGFR) play an important role in protecting joint tissues from OA. EGF, as a ligand of EGFR, has been shown to be abundant in normal cartilage tissues [11]. However, direct and prompt injection of EGF to chronic inflammation in joint tissues could not be a feasible therapeutic approach due to the short half-life of EGF [12]. Therefore, a sustained and localized delivery of EGF in a spatial-temporally fashion is needed as a potential treatment of osteoarthritis.

Microencapsulation of a given drug with chitosan has been demonstrated to be a feasible delivery approach in nanomedicine. Chitosan could be obtained from chemical treatment of sodium hydroxide or enzymatic deacetylation [13, 14]. Chitosan-based delivery is particularly suitable for local administration, such as bronchitis or vaginal mucosa as well as dermis [15]. Moreover, the chitosan-formed nanoparticles can be adjusted in size, ranging from 10–1000 nm [16, 17], and improve the bioavailability for water-insoluble natural products, such as flavonoids [18]. Here, we utilized polysaccharide-based chitosan to encapsulate rhEGF, supposed to prevent the degradation of rhEGF following administration *in vivo* and investigated the benefits of microencapsulation of rhEGF with HA as an excipient could be a novel approach in alleviation of OA. Ultimately, we attempted to demonstrate potential applications of bioactive components via this encapsulation technology.

2. Material and Methods

2.1. Preparation of Chitosan-Microencapsulated Recombinant Human Epidermal Growth Factor (Me-rhEGF). Chitosan was generated from deacetylation of chitin followed by protonation of amino acid groups in an acidic environment [14]. rhEGF was added to the chitosan solution with pH 4.6–6, and then the solution was adjusted to pH 6–8. Protonated chitosan became water-soluble and easily interacted and stabilized with the negatively charged rhEGF to form particles (provided by GoodCare-Biotech, Ltd., Taipei, Taiwan, and patented by JOYCOM BIO-CHEM Co., Ltd.) [19, 20].

2.2. Animals. Six-week-old male Sprague-Dawley rats, weighted from 200 to 300 g, were purchased from the National Laboratory Animal Center (Taipei, Taiwan) and maintained in the National Chung Hsing University (NCHU) Animal Experiment Research Center following the guide for the care and use of laboratory animals. These animals were provided with sterilized and unlimited chow and water and the experimental protocol was approved by the IACUC of NCHU (Approval no. 107-011).

2.3. Induction of OA and Treatments. Monosodium iodoacetate (Sigma, St. Louis, MO, USA) was used to induce OA as described previously [21]. In brief, 1.5 mg of monosodium iodoacetate was dissolved in 30 μ L of 0.9% saline followed by a single intra-articular injection into the right knee joint per mouse; control mice were given a single injection of 0.9% saline. Treatments, HA, rhEGF, or HA/Me-rhEGF were also given to each group of rats ($n=5$) on day 3 and 14 of the experiment duration via intra-articular administration within two weeks after injection of monosodium iodoacetate. Physiological and pathological changes were examined and determined by 4th week after injection of monosodium iodoacetate (Figure 1).

2.4. Pathological and Histological Analyses of Joint Tissues. The sizes and microstructure of joint tissues were measured or examined with a calibrated digital caliper (Mitutoyo, Kawasaki, Japan) and hematoxylin and eosin (H&E) staining, respectively. Briefly, tissue sections were prepared following the sacrifice on the 4th week. 5 micron sections of paraffin-impregnated tissues were subjected to H&E staining or safranin O-fast green staining (Sigma, St. Louis, MO) followed by examination of tissue structure and graded using a modified Mankin scoring system [22]. The final scores correlated with higher joint tissue destruction.

2.5. Analyses for Serum Biomarkers. Rat blood was collected at 4 weeks after rats were sacrificed. Rat blood samples were centrifugated at $1500 \times g$ for 10 min to obtain serum. The concentrations of nitric oxide (NO) were determined by Griess assay to quantify the oxidation product of NO, nitrite [23]. Briefly, 100 μ M of sodium nitrate and Griess reagent (equal volumes of 2% sulfanilamide and 0.2% N-(1-

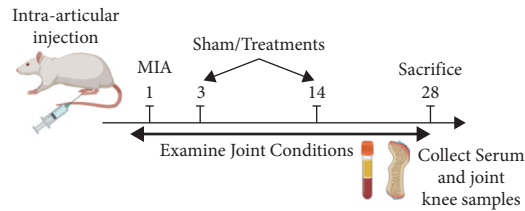


FIGURE 1: Schematic illustration of experimental design.

naphthyl)ethylenediamine dihydrochloride) were added to a well in a 1 : 1 ratio followed by incubation for 10 min at room temperature and measurement at 540 nm by an ELISA reader.

Prostaglandin E2 (PGE2; Cusabio, Biotech, Wuhan, Hubei, China), proinflammatory cytokines, including IL-1 β , IL-6, IL-17A, and TNF- α (Thermo Fisher Scientific, Waltham, MA, USA), and cartilage degeneration mediators, cartilage oligomeric matrix protein (COMP) (Cusabio), and c-terminal cross-linked telopeptides of type II collagen (CTX-II) (Lifespan Biosciences Corporations, Seattle, WA, USA) were determined by indicated ELISA kits. 100 μ L of diluted serum (50 μ L/well for PGE2 kit) was added to wells coated with capture antibodies and blocked with 5% BSA blocking buffer for 2 hrs followed by washing with PBS-T buffer (0.5% Tween-20 in PBS), 100 μ L/well biotinylated detection antibody for 1 h, and 100 μ L/well Avidin-HRP for 30 min at room temperature. Finally, 100 μ L/well TMB substrate was used to develop the colorimetric reaction which lastly measured by an ELISA reader at 450 nm after the reactions were terminated by ELISA stop solution (100 μ L/well of 0.16 M sulfuric acid).

2.6. Western Blot Analysis. The homogenates of rat cartilages were centrifuged twice at 12000 $\times g$ for 15 min at 4°C to isolate supernatant followed by quantification using a BCA Protein Assay Kit (Bio-Rad, Hercules, CA) and western blotting as described previously [24]. In brief, protein lysates were separated by SDS-PAGE and transferred to polyvinylidene fluoride (PVDF) membranes. The membranes were incubated with a blocking buffer (5% nonfat milk in Tris-buffered saline and Tween-20) followed by incubating with the following antibodies at 1 : 1000 dilutions: iNOS, COX-2, MMP-3, MMP-7, and GAPDH (all from Abcam, Cambridge, MA, USA) for overnight at 4°C. A 1 : 1000 dilution of goat-anti-rat IgG-conjugated with horseradish peroxidase (HRP; cat. no. 111-35-114; Jackson ImmunoResearch Laboratories, West Grove, PA, USA) secondary antibody was added to membranes for a 1-hour incubation. Protein detection was performed using an ECL Western Blotting Substrate Kit (ECL Prime Western Blotting Substrate; GE Healthcare Life Sciences, Piscataway, NJ, USA) and by imaging using the Hansor Luminescence Image System (Taichung, Taiwan). All the densitometric analysis for western blotting results was conducted using ImageJ v1.47 (Bethesda, MD, USA).

2.7. Prediction of Protein-Protein Interaction. Osteoarthritis-related proteins (DOID: 8398) were extracted from Human Disease Ontology database ([\[ontology.org/\]\(https://disease-ontology.org/\)\) via R package “Dose.” Protein-protein interactions network was constructed by R package “STRINGdb” and “Cytoscape” with interaction score = 0.9.](https://disease-</p>
</div>
<div data-bbox=)

2.8. Statistics. All data were plotted as mean \pm SEM unless stated elsewhere. The statistical significance between groups was defined as *P* value < 0.05 using the student’s *t*-test or one-way ANOVA with subsequent Tukey’s HSD test with Prism v8.4 (GraphPad Inc., La Jolla, CA, USA).

3. Results and Discussion

By applying the microencapsulation technology mentioned earlier, we obtained the microencapsulated rhEGF for the entire study. Before ensuring the integrity structure of rhEGF, we utilized transmission electron microscope (TEM) to visualize the microencapsulated rhEGF. As shown in Figure 2, these microspheres were well-preserved in the polysaccharide (chitosan) shell with the sizes around dozens of nanometers, ranging from 50–200 nm.

We then prompted to determine whether HA, rhEGF, or HA/Me-rhEGF could elicit any protective effects to ameliorate osteoarthritic symptoms in an animal model; we utilized monosodium iodoacetate (MIA), a selective inhibitor of glyceraldehyde-3-phosphate dehydrogenase, to induce osteoarthritis-like symptoms on rats. On 14 days of administration of MIA, animals exhibited swollen knees (Figure 3(a); MIA group). This was characterized with the pathological changes in the tissue microstructures, including clefts and irregular surfaces, a loss of proteoglycan (safranin-O staining) and cartilage, and elevated total Mankin scores (Figures 3(b) and 3(c); MIA group). Individual use of HA or rhEGF reduced the severity of OA in rats, but not significantly. The administration of HA/Me-rhEGF, in contrast, resulted in drastic decreases of knee swelling and stymied overall OA symptoms (Figures 3(a)–3(c); HA/Me-rhEGF group), demonstrating the protective effects of combined treatment with HA/Me-rhEGF.

Levels of cartilage oligomeric protein (COMP) and C-telopeptide of type II collagen (CTX-II) in circulation are highly associated with the cartilage degradation and pathogenesis of OA [25]. Keeping this in mind, we quantified the concentrations of COMP and CTX-II in rat serum by ELISA. Levels of COMP among groups corresponded to the severity seen in histological evidences. On the other hand, the circulating level of CTX-II in rhEGF treatment group was barely inhibited and was not suppressed as effectively as seen in groups treated with only HA or HA/Me-rhEGF (Figure 3(d)). To further pin down the downstream protein

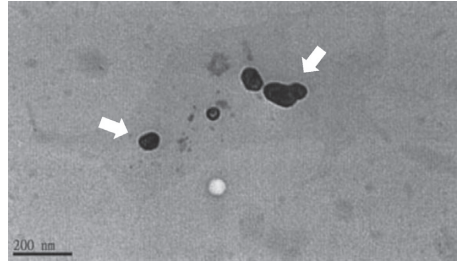


FIGURE 2: Image of chitosan-microencapsulated rhEGF from transmission electronic microscope (TEM).

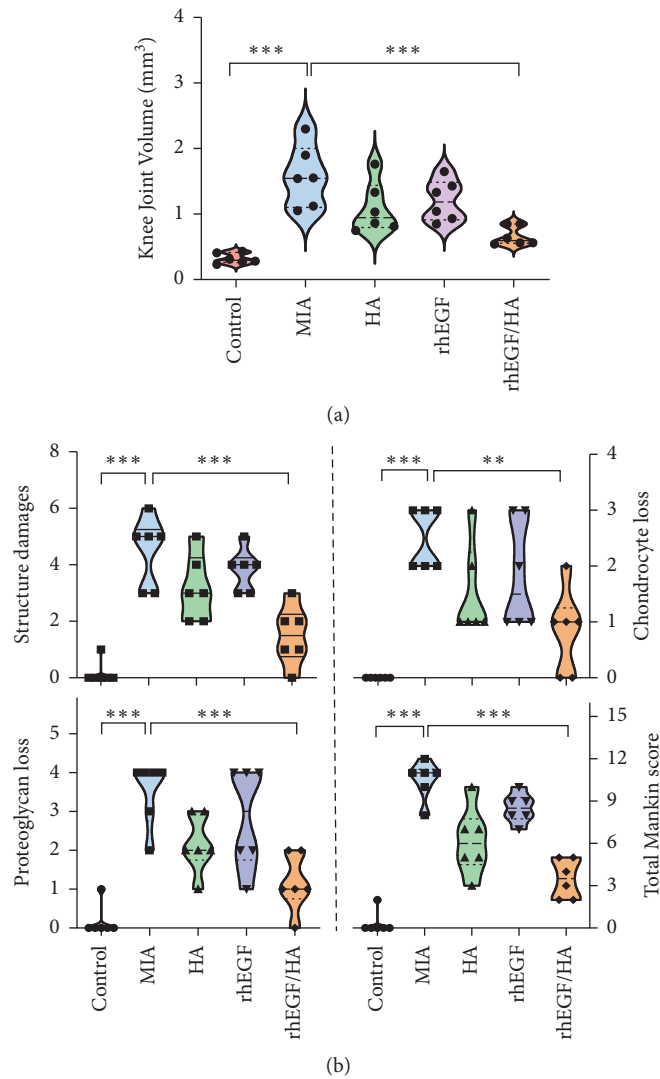


FIGURE 3: Continued.

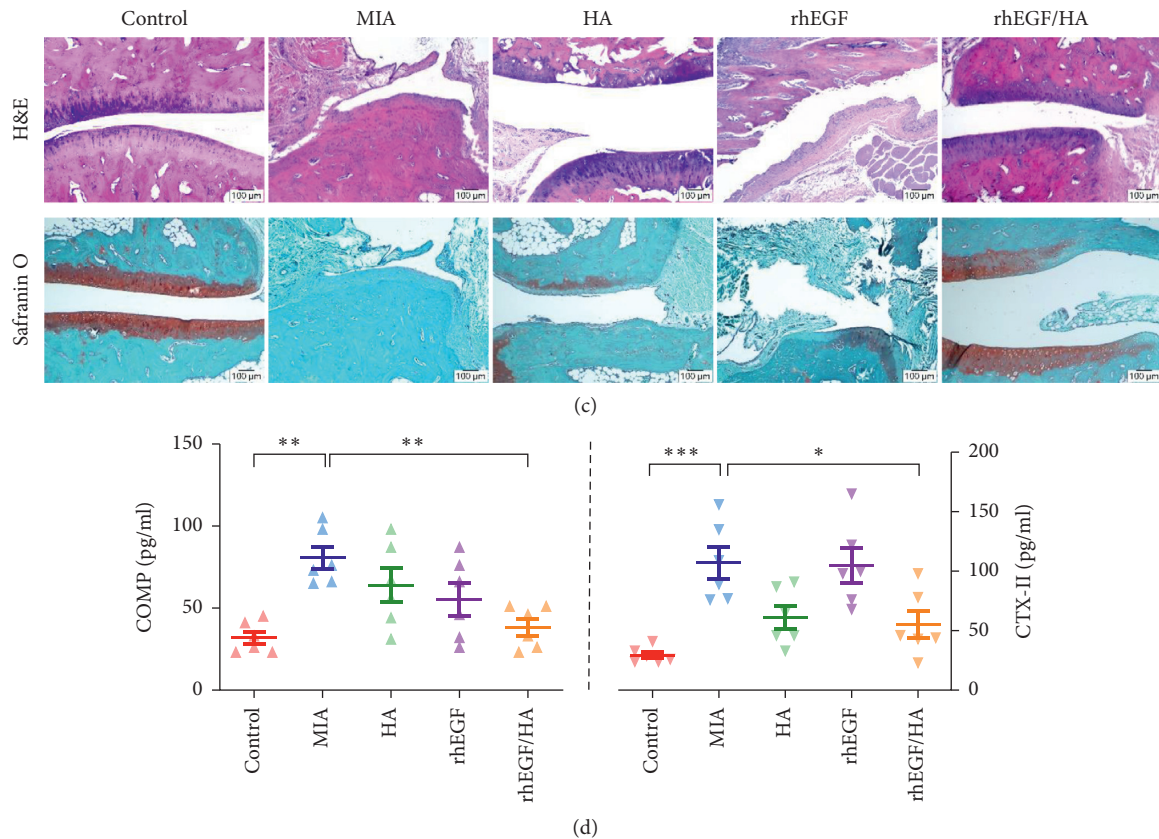


FIGURE 3: Effects of HA, rhEGF, and HA/Me-rhEGF on MIA-induced OA rats. (a) Sizes of knee joints measured by a knee diameter, and (b) joint lesions, including destructive tissue structure, chondrocyte and cartilage loss, and total Mankin grades, were examined and are presented as mean \pm SEM. (c) Representative images of histological alterations in the knee joints as indicated by H&E staining and safranin O/fast green staining. (d) COMP and CTX-II in serum were measured by ELISA as cartilaginous degradation indicators (mean \pm SEM from three independent experiments).

expressions which could be related to osteoarthritis and prominently influenced by our designated treatments, HA, rhEGF, or HA/Me-rhEGF, we constructed the protein-protein interaction network following extraction of osteoarthritis-related proteins from Human Disease Ontology database. As highlighted in Figure 4, the inflammatory mediators, cytokines, and matrix metalloproteinases appeared to be worthwhile for further examinations.

As such, we investigated whether osteoarthritic inflammation was also alleviated by the treatments by examining the proinflammatory mediators and cytokines, such as prostaglandin E2 (PGE2), nitric oxide (NO), IL-1 β , IL-6, TNF- α , and IL-17A. The data shown in Figure 5(a) were consistent with the histopathological changes shown in Figure 3 where the treatment of HA/Me-rhEGF reduced the circulating levels of proinflammatory mediators significantly. Despite the similar trends, the treatment of HA or rhEGF did not significantly result in lowered levels of proinflammatory cytokines, as was seen in combinational treatment.

Next, we evaluated the inflammatory mediators, particularly nitric oxide (NO) and prostaglandin E2 (PGE2) in serum and the changes of corresponding upstream signaling pathways via ELISA and western blot, respectively. Our data indicated that concentrations of

NO and PGE2 in osteoarthritic rats were remarkably increased. In comparison, the individually administered HA or rhEGF specimens displayed a slight reduction of inflammatory mediators, and HA/Me-rhEGF treatment still showed the most significant reduction of aforementioned inflammatory mediators (Figure 5(b)). Moreover, the expressions of inducible nitric oxide synthase (iNOS) and cyclooxygenase-2 (COX-2) responsible for generation of NO and PGE2, respectively, were also downregulated in the cartilaginous tissues (Figure 6(a)). These data were consistent with the data obtained from ELISA. Our results suggest that HA/Me-rhEGF was efficiently able to reduce the inflammation in osteoarthritic rats.

Finally, we attempted to examine the protein levels of matrix metalloproteinase (MMPs) which could be closely associated with the pathogenesis of OA and some of them are known as therapeutic targets for OA [26, 27]. As our results show, the expression of MMP-3 and MMP-13 in OA rats was profoundly upregulated and, surprisingly, the administration of HA or rhEGF independently did not diminish levels of MMP-3 and MMP-13. However, the treatment of HA/Me-rhEGF reduced the level of MMP-3 remarkably as well as MMP-13 to some extent despite not

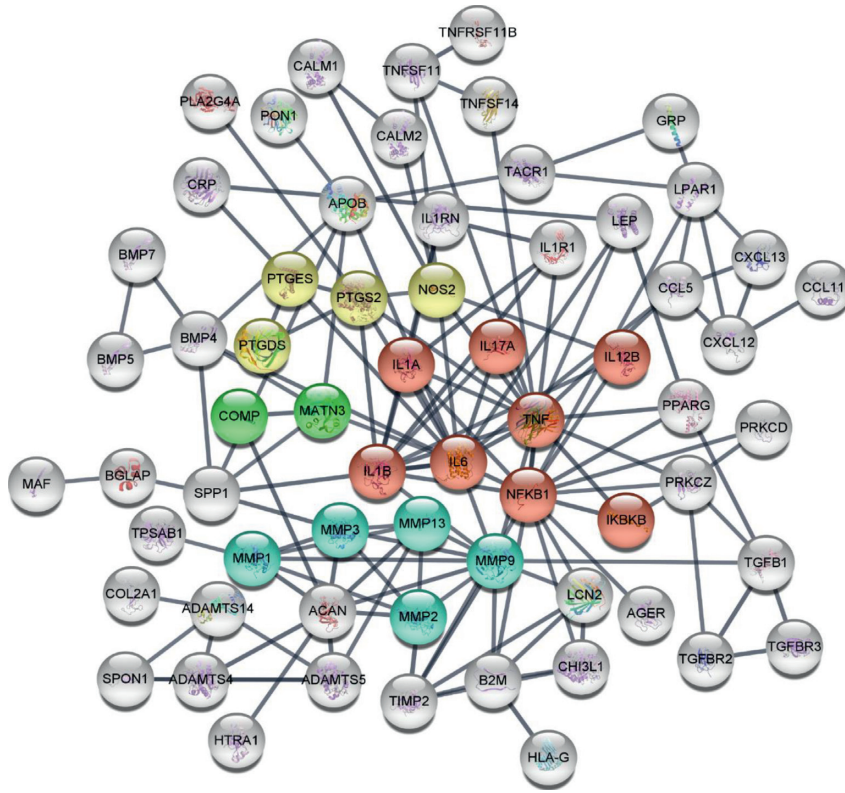
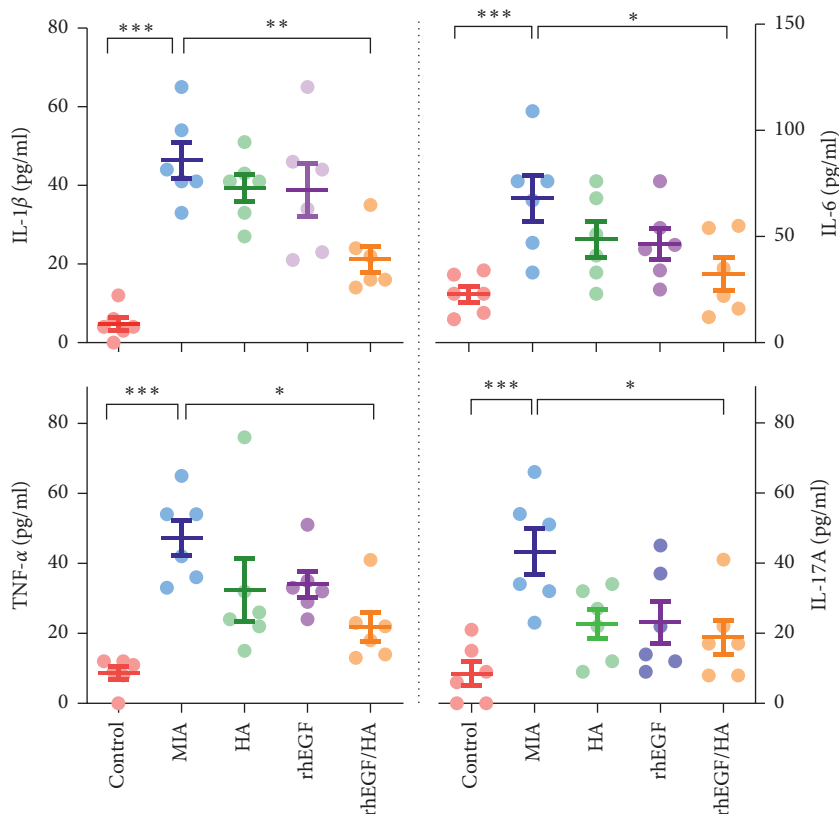


FIGURE 4: Prediction of osteoarthritis-related protein-protein interaction. The proteins were extracted from Human Disease Ontology database and the network was constructed by R packages. Color red designates inflammatory responses; yellow indicates the inflammatory mediators; green means osteoarthritis indication-related proteins; and blue means MMP cascade.



(a)
FIGURE 5: Continued.

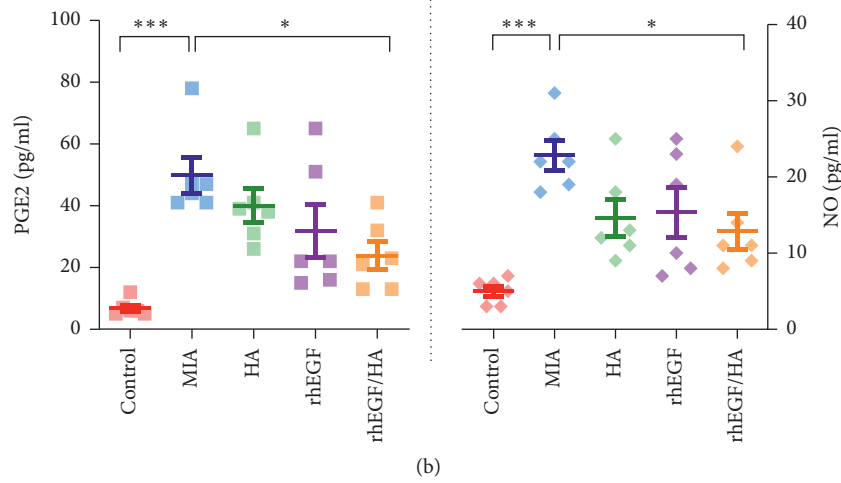


FIGURE 5: Inflammatory cytokines in circulating serum. The levels of (a) IL-1 β , IL-6, TNF- α , and IL-17A and (b) inflammatory mediators, prostaglandin E2 (PGE2), and nitric oxide (NO) in serum samples were measured by ELISA or Griess reaction (NO) with or without treatments of HA, rhEGF, or HA/Me-rhEGF. Data are expressed as mean \pm SEM from the three independent experiments.

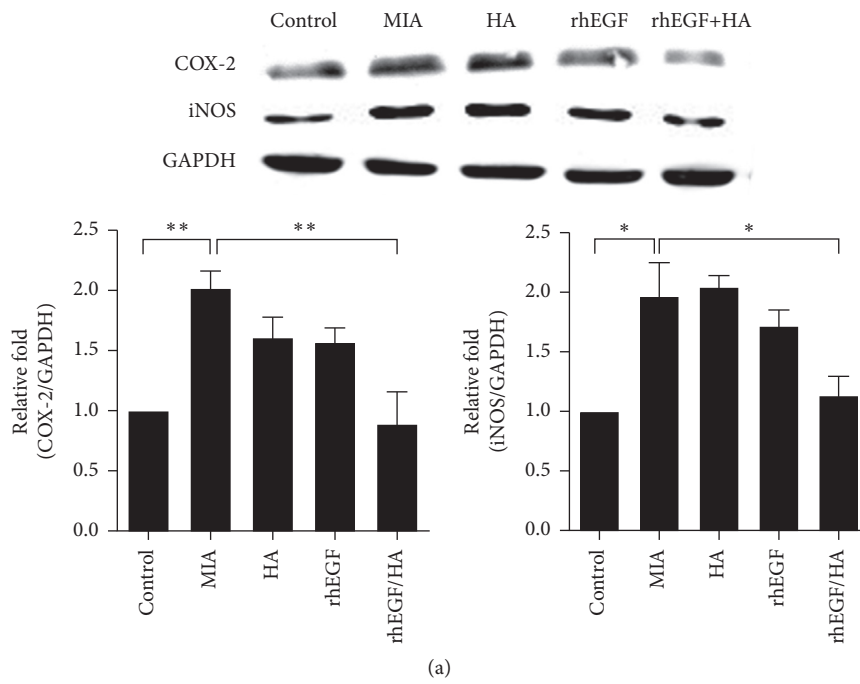


FIGURE 6: Continued.

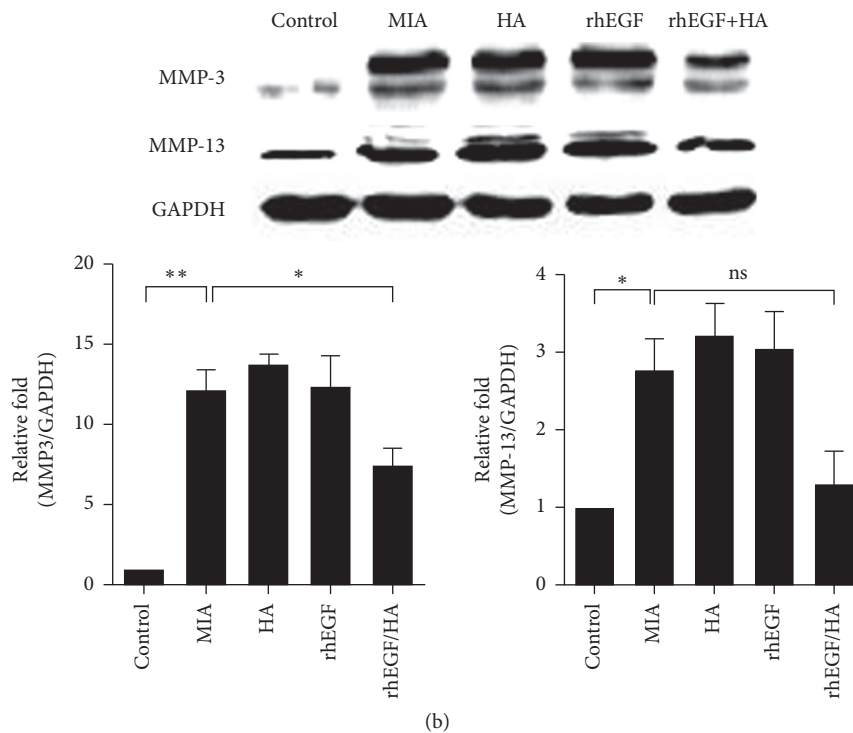


FIGURE 6: Effect of treatments on inflammatory mediators and MMPs in cartilaginous tissues. The expressional levels of (a) iNOS and COX-2 and (b) MMP-3 and MMP-13 were determined by western blot analyses in joint homogenates. GAPDH was used as a loading control, and protein expressions were quantified by ImageJ software and normalized based on GAPDH expression. Data are expressed as mean \pm SEM from the three independent experiments.

significantly (Figure 6(b)), suggesting the administration of HA/Me-rhEGF could efficiently alleviate the MIA-induced OA through inhibition of MMP cascade.

Overall, our results indicate that direct administration of HA or rhEGF via intra-articular injection could partially ameliorate the pathological indexes of osteoarthritis induced with MIA, such as inflammatory mediators, NO and PGE₂, and proinflammatory cytokines, but a significant effect was achieved upon treating with HA and chitosan-microencapsulated rhEGF. In addition to the combinational efficacy, we demonstrated that the two dosages of HA/Me-rhEGF prolonged the therapeutic duration in the MIA-induced OA model (Figure 3) compared to previous studies where at least three times of HA injections were required to observe the symptomatic alleviation in OA rats [28, 29], signifying the possibility to reduce the revisiting frequency for OA patients.

Despite the benefits of HA administration in OA, we observed that the HA combined with rhEGF were far more effective to stymie the arthritic symptoms. CD44 was shown to be the receptor of HA [30] and the expression level of CD44 on the articular cartilage was also highly associated with the severity of OA [31]; the binding of CD44 and HA inhibited the release of interleukin-1 β and MMPs, including MMP-3 and 13 (Figures 5(a) and 6(b)) [32]. Despite potential benefits of HA, it is noted that HA alone is not able to substantially improve the lubricating condition in a joint cavity [6, 7, 9]. The lubrication effect mainly comes from the aggregation of glycoprotein in the

extracellular matrix (ECM) [33], where EGF serves as a core protein to facilitate the glycoprotein aggregation in the joint cavity. In fact, such glycoprotein aggregations require the interaction between HA and EGF, which could further be cross-linked with fibulins in ECM and ultimately form protein-glycosaminoglycan complexes to provide necessary lubrication and harmonious physical status in joint tissues [34, 35]. Hence, HA and rhEGF could synergistically facilitate the improvement of OA conditions.

In conclusion, OA is a chronic inflammatory disease that is difficult to be completely treated. However, our study provides insight and promising results for the prompt delivery of HA/Me-rhEGF. Our novel therapeutic approach ensures a steady and consistent release of rhEGF coordinating with HA to ameliorate the symptoms of MIA-induced OA in rats. That is evidenced by significantly reduced inflammatory cytokines and mediators. Overall, chitosan-microencapsulated rhEGF exhibited higher stability in preservation and provided better anti-inflammatory effect than nonencapsulated rhEGF. As a result, we believe that this HA/Me-rhEGF has promising potential as an OA treatment in the clinical field.

Data Availability

The data used to support the findings of this study are included within the article.

Disclosure

The authors received no financial support for the research, authorship, and/or publication of this article.

Conflicts of Interest

The authors declare that there are no conflicts of interest.

Acknowledgments

The authors thank Dr. Hsien-Tzu Chen for comments on this manuscript.

References

- [1] S. Glyn-Jones, A. J. R. Palmer, R. Agricola et al., "Osteoarthritis," *The Lancet*, vol. 386, no. 9991, pp. 376–387, 2015.
- [2] J. Riegger, M. Rehm, G. Büchele et al., "Serum cartilage oligomeric matrix protein in late-stage osteoarthritis: association with clinical features, renal function, and cardiovascular biomarkers," *Journal of Clinical Medicine*, vol. 9, 1 page, 2020.
- [3] J. Bjordal, "NSAIDs in osteoarthritis: irreplaceable or troublesome guidelines?" *British Journal of Sports Medicine*, vol. 40, no. 4, pp. 285–286, 2006.
- [4] M. F. Rai and C. T. Pham, "Intra-articular drug delivery systems for joint diseases," *Current Opinion in Pharmacology*, vol. 40, pp. 67–73, 2018.
- [5] P. Vincent, "Intra-articular hyaluronic acid in the symptomatic treatment of knee osteoarthritis: a meta-analysis of single-injection products," *Current Therapeutic Research*, vol. 90, pp. 39–51, 2019.
- [6] E. L. Radin, D. A. Swann, and P. A. Weisser, "Separation of a hyaluronate-free lubricating fraction from synovial fluid," *Nature*, vol. 228, no. 5269, pp. 377–378, 1970.
- [7] P. Richette, P. Ravaut, T. Conrozier et al., "Effect of hyaluronic acid in symptomatic hip osteoarthritis: a multicenter, randomized, placebo-controlled trial," *Arthritis & Rheumatism*, vol. 60, no. 3, pp. 824–830, 2009.
- [8] E. Fouissac, M. Milas, and M. Rinaudo, "Shear-rate, concentration, molecular weight, and temperature viscosity dependences of hyaluronate, a wormlike polyelectrolyte," *Macromolecules*, vol. 26, no. 25, pp. 6945–6951, 1993.
- [9] J. Klein, "Molecular mechanisms of synovial joint lubrication," *Proceedings of the Institution of Mechanical Engineers - Part J: Journal of Engineering Tribology*, vol. 220, no. 8, pp. 691–710, 2006.
- [10] F. Eymard, P. Ornetti, J. Maillet et al., "Intra-articular injections of platelet-rich plasma in symptomatic knee osteoarthritis: a consensus statement from French-speaking experts," *Knee Surg Sports Traumatol Arthrosc*, 2020.
- [11] X. Zhang, V. A. Siclari, S. Lan et al., "The critical role of the epidermal growth factor receptor in endochondral ossification," *Journal of Bone and Mineral Research*, vol. 26, no. 11, pp. 2622–2633, 2011.
- [12] D. P. Calnan, A. Fagbemi, J. Berlanga-Acosta et al., "Potency and stability of C terminal truncated human epidermal growth factor," *Gut*, vol. 47, no. 5, pp. 622–627, 2000.
- [13] M. N. V. Ravi Kumar, "A review of chitin and chitosan applications," *Reactive and Functional Polymers*, vol. 46, no. 1, pp. 1–27, 2000.
- [14] C. Lim, D. W. Lee, J. N. Israelachvili, Y. Jho, and D. S. Hwang, "Contact time- and pH-dependent adhesion and cohesion of low molecular weight chitosan coated surfaces," *Carbohydrate Polymers*, vol. 117, pp. 887–894, 2015.
- [15] M. Hasanifard, B. Ebrahimi-Hosseinzadeh, A. Hatamian-Zarmi, A. H. Rezayan, and M. A. Esmaili, "Development of thiolated chitosan nanoparticles based mucoadhesive vaginal drug delivery systems," *Polymer Science - Series A*, vol. 59, no. 6, pp. 858–865, 2017.
- [16] A. Ghadi, S. Mahjoub, F. Tabandeh, and F. Talebnia, "Synthesis and optimization of chitosan nanoparticles: potential applications in nanomedicine and biomedical engineering," *Caspian journal of internal medicine*, vol. 5, no. 3, pp. 156–161, 2014.
- [17] M. Khanmohammadi, H. Elmizadeh, and K. Ghasemi, "Investigation of size and morphology of chitosan nanoparticles used in drug delivery system employing chemometric technique," *Iranian Journal of Pharmaceutical Research: IJPR*, vol. 14, no. 3, pp. 665–675, 2017.
- [18] M. A. Mohammed, J. T. M. Syeda, K. M. Wasan, and E. K. Wasan, "An overview of chitosan nanoparticles and its application in non-parenteral drug delivery," *Pharmaceutics*, vol. 9, no. 4, p. 53, 2017.
- [19] F. Andrade, F. Goycoolea, D. A. Chiappetta, J. das Neves, A. Sosnik, and B. Sarmento, "Chitosan-grafted copolymers and chitosan-ligand conjugates as matrices for pulmonary drug delivery," *International Journal of Carbohydrate Chemistry*, vol. 2011, Article ID 865704, 2011.
- [20] D. W. Lee, C. Lim, J. N. Israelachvili, and D. S. Hwang, "Strong adhesion and cohesion of chitosan in aqueous solutions," *Langmuir*, vol. 29, no. 46, pp. 14222–14229, 2013.
- [21] C. L. Marker and J. D. Pomonis, "The monosodium iodoacetate model of osteoarthritis pain in the rat," *Methods in Molecular Biology*, vol. 851, pp. 239–248, 2012.
- [22] C. Pauli, R. Whiteside, F. L. Heras et al., "Comparison of cartilage histopathology assessment systems on human knee joints at all stages of osteoarthritis development," *Osteoarthritis and Cartilage*, vol. 20, no. 6, pp. 476–485, 2012.
- [23] L. A. Ridnour, J. E. Sim, M. A. Hayward et al., "A spectrophotometric method for the direct detection and quantitation of nitric oxide, nitrite, and nitrate in cell culture media," *Analytical Biochemistry*, vol. 281, no. 2, pp. 223–229, 2000.
- [24] S. P. Wang, S. C. Lin, S. Li, Y. H. Chao, G. Y. Hwang, and C. C. Lin, "Potent antiarthritic properties of phloretin in murine collagen-induced arthritis," *Evidence-based Complementary and Alternative Medicine*, vol. 2016, Article ID 9831263, 2016.
- [25] B. Bai and Y. Li, "Combined detection of serum CTX-II and COMP concentrations in osteoarthritis model rabbits: an effective technique for early diagnosis and estimation of disease severity," *Journal of Orthopaedic Surgery and Research*, vol. 11, no. 1, p. 149, 2016.
- [26] J.-J. Chen, J.-F. Huang, W.-X. Du, and P.-J. Tong, "Expression and significance of MMP3 in synovium of knee joint at different stage in osteoarthritis patients," *Asian Pacific Journal of Tropical Medicine*, vol. 7, no. 4, pp. 297–300, 2014.
- [27] Q. Hu and M. Ecker, "Overview of MMP-13 as a promising target for the treatment of osteoarthritis," *International Journal of Molecular Sciences*, vol. 22, no. 4, Article ID 1742, 2021.
- [28] M. Ikeuchi, M. Izumi, K. Aso, N. Sugimura, T. Kato, and T. Tani, "Effects of intra-articular hyaluronic acid injection on immunohistochemical characterization of joint afferents in a rat model of knee osteoarthritis," *European Journal of Pain*, vol. 19, no. 3, pp. 334–340, 2015.

- [29] S. Jimbo, Y. Terashima, A. Teramoto et al., “Antinociceptive effects of hyaluronic acid on monoiodoacetate-induced ankle osteoarthritis in rats,” *Journal of Pain Research*, vol. 12, pp. 191–200, 2019.
- [30] D. S. Bhattacharya, D. Svechkarev, J. J. Soucek et al., “Impact of structurally modifying hyaluronic acid on CD44 interaction,” *Journal of Materials Chemistry B*, vol. 5, no. 41, pp. 8183–8192, 2017.
- [31] F.-J. Zhang, W. Luo, S.-G. Gao et al., “Expression of CD44 in articular cartilage is associated with disease severity in knee osteoarthritis,” *Modern Rheumatology*, vol. 23, no. 6, pp. 1186–1191, 2013.
- [32] R. Altman, A. Manjoo, A. Fierlinger, F. Niazi, and M. Nicholls, “The mechanism of action for hyaluronic acid treatment in the osteoarthritic knee: a systematic review,” *BMC Musculoskeletal Disorders*, vol. 16, no. 1, p. 321, 2015.
- [33] E. Ruoslahti, “Brain extracellular matrix,” *Glycobiology*, vol. 6, no. 5, pp. 489–492, 1996.
- [34] P. J. Roughley and J. S. Mort, “The role of aggrecan in normal and osteoarthritic cartilage,” *Journal of experimental orthopaedics*, vol. 1, no. 1, Article ID 8, 2014.
- [35] L. Ma, A. Gaisinskaya-Kipnis, N. Kampf, and J. Klein, “Origins of hydration lubrication,” *Nature Communications*, vol. 6, no. 1, Article ID 6060, 2015.